Efficient Hit-to-Lead Searching of Kinase Inhibitor Chemical Space via Computational Fragment Merging

Grigorii V. Andrianov[1,2], Wern Juin Gabriel Ong[1,3], Ilya Serebriiskii[1,2], and John Karanicolas[1*]

[1] Program in Molecular Therapeutics, Fox Chase Cancer Center, Philadelphia, PA 19111-2497

[2] Institute of Fundamental Medicine and Biology, Kazan Federal University, Kazan, Russia, 420008

[3] Bowdoin College, Brunswick, ME 04011

*To whom correspondence should be addressed. E-mail: **john.karanicolas@fccc.edu**, 215-728-7067

Abstract

In early stage drug discovery, the stage of hit-to-lead optimization (or "hit expansion") entails starting from a newly-identified active compound, and improving its potency or other properties. Traditionally this process relies on synthesizing and evaluating a series of analogs to build up structure-activity relationships. Here, we describe a computational strategy focused on kinase inhibitors, intended to expedite the process of identifying analogs with improved potency. Our protocol begins from an inhibitor of the target kinase, and generalizes the synthetic route used to access it. By searching for commercially-available replacements for the individual building blocks used to make the parent inhibitor, we compile an enumerated library of compounds that can be accessed using the same chemical transformations; these huge libraries can exceed many millions – or billions – of compounds. Because the resulting libraries are much too large for explicit virtual screening, we instead consider alternate approaches to identify the top-scoring compounds. We find that contributions from individual substituents are well-described by a pairwise additivity approximation, provided that the corresponding fragments position their shared core in precisely the same way relative to the binding site. This key insight allows us to determine which fragments are suitable for merging into a single new compounds, and which are not. Further, the use of the pairwise approximation allows interaction energies to be assigned to each compound in the library, without the need for any further structure-based modeling: interaction energies instead can be reliably estimated from the energies of the component fragments. We demonstrate this protocol using libraries built from five representative kinase inhibitors drawn from the literature, which target four different kinases: CDK9, CHK1, CDK2, and ACK1. In each example, the enumerated library includes additional analogs reported by the original study to have activity, and these analogs are successfully prioritized within the library. We envision that the insights from this work can facilitate the rapid assembly and screening of increasingly large libraries for focused hit-to-lead optimization. To encourage adoption of these methods and enable further analyses, we disseminate the computational tools needed to deploy this protocol.

Introduction

The practice of virtual screening has historically comprised two separate and complementary tasks, irrespective of a campaign's particular target or goals. The first task focuses on finding active compounds ("hits") by rapidly docking a large collection of drug-like compounds against some protein target [1]. The second task aims to take the validated screening hits, irrespective of whether they were obtained by computational or biochemical screens, and to optimize their activity by proposing improved analogs [2,3].

Conceptually, these two steps are sharply delineated. The former task seeks to sample chemical space as broadly as possible, thus requiring fast and approximate methods for evaluating each compound. For many years it was general practice to screen the ubiquitous ZINC database (a concatenation of numerous vendor's catalogs that spanned 3-8 million diverse compounds) [4,5] in search of those worth purchasing and testing for activity. By contrast, the second task acknowledges that discerning differences between compounds requires careful and expensive detailed simulations, which even then can provide reliable comparisons only between closely related compounds; thus, this task has been confined to searching a highly focused part of chemical space. Comparisons have typically been carried out via free energy perturbation methods (or equivalent), applied at the scale of about a hundred compounds [6].

In the past few years, however, several key developments have blurred the delineation between these two tasks; these developments have further prompted the community to completely re-think how computers might best provide new chemical matter for a target of interest. The first and most cataclysmic change arose when certain chemical vendors began listing not just the contents of their shelves, but also enumerating all the compounds that can be readily synthesized from these building blocks [7]. Enabled by robots carrying out simple and robust chemical transformations, compounds from these "make-on-demand" collections can often be supplied more quickly and cheaply than historical virtual screening hits.

Just as importantly though, the coverage of chemical space from make-on-demand collections is also fundamentally different from the historically-biased compounds previously housed in the ZINC database. Because the chemical transformations that underlie these new collections are restricted to those

efficiently carried out in automated synthetic protocols, the resulting chemical space is less diverse than ZINC's historical offerings. Instead, variants of a given chemical scaffold are proffered in which a given building block may be replaced with thousands of related alternatives: thus, these new collections afford incredibly *dense* coverage of chemical space. This fundamental difference in how chemical diversity is accumulated by enumerating reactions was recognized well before the advent of these new collections, and was found to be the case upon designing a virtual library of one-pot synthetically-accessible compounds to mimic amino acid sidechains in protein-protein interfaces [8].

The sheer size of these make-on-demand collections – now about 19 billion compounds – has forced practitioners to reconsider how this chemical space should be sampled, given the impracticality of sequentially docking this many compounds to one's target protein. One potential approach might be to screen a diverse subset of the collection, with the goal of identifying useful scaffolds, then subsequently re-screen each of the available compounds that elaborate this scaffold in different ways [9]. However, two separate studies have by now demonstrated that valuable hits would be missed this way: one cannot necessarily recognize from the scaffold alone that an elaborated analog might score well [7,9].

While we do not yet offer a solution for the overarching problem of how to best navigate a target-agnostic collection of 19 billion unrelated compounds, here we address a narrower but equally-pressing question. For certain well-studied target classes, clusters of "privileged" chemotypes have been identified. This is especially true in the case of protein kinases, where the structurally-conserved ATP-binding site has led to the repeated re-use (or inadvertent re-discovery) of a broad set of hinge-binding cores [10]. By starting from a given core and choosing different substituents, a particular core can be developed in different ways; thus, selective inhibitors for many different kinases can be built from the same core [11]. This insight further serves as the basis for synthesis of numerous kinase-focused chemical libraries [12], which harbor a limited diversity of chemotypes but are poised to be optimized for any kinase of interest.

The underlying challenge we tackle here, then, is how one might efficiently search the narrow but very dense swath of chemical space around a given core, to optimize it for a particular target. We choose five diverse inhibitors of different kinases as starting points, and in each case generate and explore the

chemical space around this inhibitor. We describe a "deconstruction-reconstruction" approach [13,14], in which the synthetic route used to build the known inhibitor is generalized, and used to create a huge chemical library that densely samples synthetically-accessible chemical space. We find that by adapting strategies that underlie fragment merging [15,16], the top-scoring compounds from the resulting library can be identified in an extremely efficient manner.

Computational Approach

Protein kinases are a thoroughly established class of targets for therapeutic intervention, particularly in oncology, due in part to their central role in mediating cellular signaling [17]. Since the pioneering success of imatinib twenty years ago, over 50 new kinase inhibitors have attained FDA approval, with hundreds more in development [18]. While many kinases also include an assortment of additional domains to refine their activity, all of them share a highly conserved catalytic domain (**Figure 1a**). This domain is responsible for transferring a phosphate group from ATP to a substrate protein, and in so doing altering the recipient protein's activity.

In their active conformation, all protein kinases adopt the same "DFG-in" [19] (or "BLAminus" [20]) structure. This conformation engages ATP in a specific pose, using a set of nearly invariant interactions; accordingly, the ATP binding site exhibits exceedingly strong structural conservation. Most kinase inhibitors bind to this site, disrupting kinase activity by competing with ATP. The majority of these – known as "Type I" inhibitors – occupy almost exactly the same space as ATP within the binding site, and are thus compatible with the kinase's active conformation. By contrast, "Type II" inhibitors additionally occupy a secondary region of the binding site that can be accessed by displacing the kinase's DFG loop from its active conformation (shifting this loop into one of many "DFG-out" conformations).

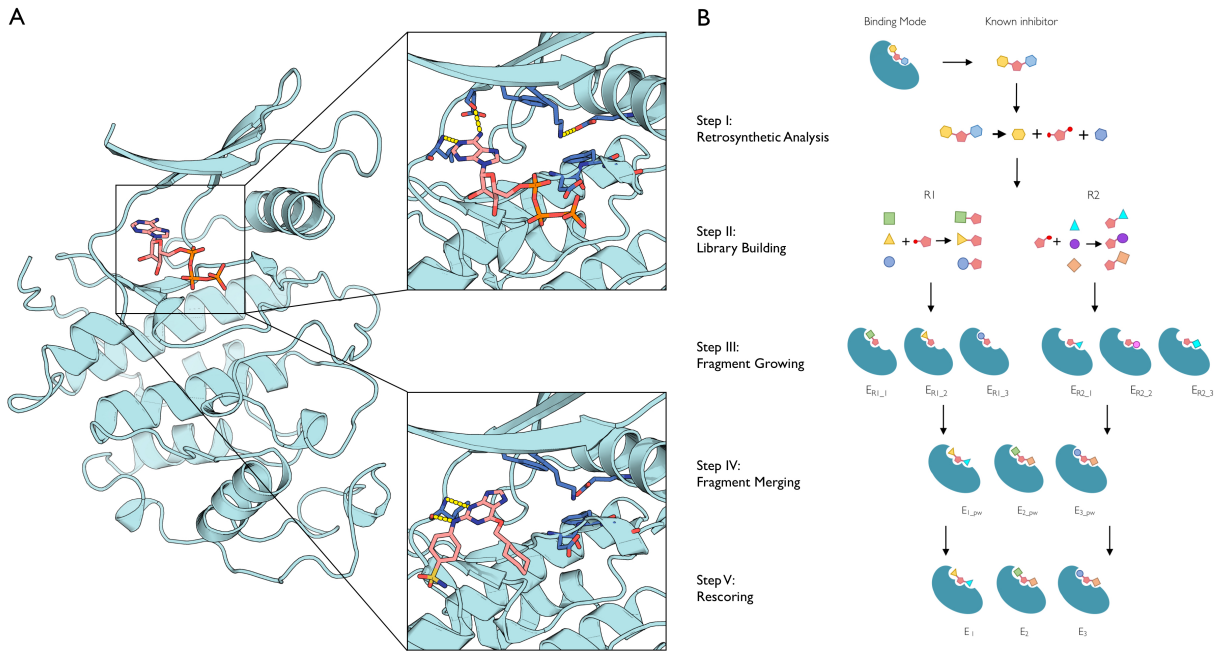

Figure 1: Computational fragment merging strategy for efficient hit-to-lead optimization of kinase inhibitors. (**A**) The catalytic domain of a representative protein kinase, cyclin-dependent kinase 2 (CDK2). Crystal structures in complex with ATP (*upper inset*) and in complex with a representative Type I inhibitor (*lower inset*) demonstrate the similarity of the protein conformation, and the inhibitor's mimicry of the interactions between ATP and the kinase. (**B**) Summary of our computational fragment merging approach. *Step I:* Starting from a known inhibitor, we use retrosynthetic analysis and its crystal structure in complex with the kinase to decompose the inhibitor into its hinge-binding motif (*pink pentagon*) and its side chains (*blue and yellow hexagons*). *Step II:* Diversity at the side chains is introduced by identifying alternate (commercially-available) building blocks that can be used in place of the original reactants. These are then joined to the hinge-binding scaffold to form newly-elaborated hinge-binding fragments. *Step III:* Each of the elaborated hinge-binding fragments are separately aligned into the kinase's ATP-binding site, and refined via energy minimization. *Step IV:* Fragments elaborated at different positions can be merged if the shared core is positioned in precisely the same orientation. Given the shared positioning of the core, the interaction energy of the merged compound can be estimated from the interaction energies of the component fragments (assuming pairwise additivity). *Step V:* The merged inhibitor is then re-refined via energy minimization, and the interaction energy calculated explicitly (without assuming pairwise additivity).

By virtue of engaging a structurally conserved binding site evolved to recognize ATP, most Type I inhibitors in fact mimic the three-dimensional used by ATP to bind the kinase. ATP's flat adenine moiety is sandwiched between hydrophobic groups above and below, and the adenine's edge forms specific hydrogen bond interactions with backbone groups on the "hinge" region that connects the N- and C-lobes of the kinase. The same can be said for nearly all Type I kinase inhibitors: though they rarely use adenine

itself, they instead use alternate flat rings that present a comparable pattern of polar groups on their hinge-facing edge, allowing them to engage the kinase in a manner very reminiscent of ATP. Indeed, the repertoire of hinge-binding cores repeatedly used by medicinal chemists to engage kinases (mentioned earlier) form the basis for nearly all known kinase inhibitors [10], as well as for kinase-focused chemical libraries [12].

For each of the five examples to be presented in our study, we begin with some known inhibitor of a protein kinase. We selected these particular examples by virtue of the crystal structure of these inhibitors having been solved in complex with the kinase (to allow retrospective analysis), a clear hinge-binding motif, and straightforward synthetic routes. By these criteria, many more inhibitors would also qualify; we chose these five examples for study based on their chemical diversity relative to one another.

Our task will be to build a chemical library by diversifying around this compound, and then to efficiently identify the best analogs from this library. Below, we describe an approach for rapidly carrying out this search using an approach inspired by fragment merging (**Figure 1b**). In the *Results* section, which follows the description of our computational approach, we will detail the specifics of applying this approach using these five representative cases as concrete examples.

Step I: Retrosynthetic analysis

Starting from the known inhibitor, we use retrosynthetic analysis to generalize the synthesis of this compound (**Figure 1b**, *Step I*). Computational methods for synthetic route planning have made rapid and dramatic advances in recent years [21-27], and provide a natural tool to carry out this step. That said, for the current study we have drawn inhibitors from the literature, and thus we have access to already-validated synthetic routes to access these compounds. By re-using the previously-described syntheses, we expect that many of the compounds described through the reported structure-activity relationships will also be present in our designed library, facilitating benchmarking in this analysis. For this reason, we have elected in the present study to simply re-use the synthetic routes reported in the literature for each starting compound.

Step II: Library building

The goal of our approach is not to search alternate potential hinge-binding cores, but rather to exhaustively sample elaborations of the current core. The hinge-binding motif is almost always located in the middle of the inhibitor (due to the three-dimensional architecture of the kinase binding site), and so we began by (manually) identifying this motif and keeping it fixed.

For each of the building blocks appended onto the hinge-binding motif as part of the original reaction, we sought to retain the functional group(s) needed for the chemical transformation and diversify the rest of the building block. To do so, we first wrote the simplest unsubstituted version of each building block as a SMARTS string (**Table S1**). Briefly, a SMARTS string represents a molecular pattern [28]; in our case, we use these patterns to encode an abstraction of the starting building block. Thus, the SMARTS string can serve as a query to identify other compounds that could be used in the original reaction, as a substitute for the original building block. Using each SMARTS string as a query, we then searched PubChem to identify alternate building blocks from commercial vendors that could be used for this reaction (**Figure 1b**, *Step II*), with a series of additional chemical filters on the allowed hits (**Table S2**) and restrictions on the chemical vendors to include in the search (**Table S3**).

For each of the candidate building blocks, we then used the "ChemicalReaction" functionality in RDKit [29] to assemble the product of the corresponding chemical transformation. To build the complete collection of inhibitors that can be assembled from these building blocks, we wrote SMARTS strings that encode all steps to generate the final (complete) inhibitor from an arbitrary set of building blocks. However, because we planned to primarily to evaluate each substituent separately (as will be described below), we also wrote SMARTS strings to generate a corresponding fragment (i.e., one new substituent added onto the hinge-binding core) from each building block (**Table S1**).

Step III: Fragment growing

By diversifying multiple building blocks from the original reaction and exhaustively recombining them, one can thus generate very large libraries of new compounds built on the original hinge-binding

motif, that can (in principle) be accessed using the original synthetic route. Depending on the size of the library, though, it can be prohibitive to explicitly screen these.

The positioning of the hinge-binding motif within the kinase active site is typically conserved, because these motifs form hydrogen bonds to specific backbone groups on the kinase. To provide a compatible binding mode with the kinase active site, the enumerated compounds in this chemical library must therefore be accommodated in the kinase binding site without disrupting the positioning of the hinge-binding motif.

Extending the hinge-binding motif by addition of a new group is strongly reminiscent of the "growing" approach in fragment-based drug discovery (FBDD) (or fragment-based lead discovery, FBLD) [15,16]. As with fragment growing, our task is to entails adding new groups onto the starting hit, to form additional adventitious interactions with the protein target. Indeed, the first fragment-derived drug to reach the clinic was the kinase inhibitor vemurafenib (targeting BRAF V600E) [30], designed by growing the initial hinge-binding fragment 7-azaindole [31]. Some computational approaches for fragment growing have used docking or free energy perturbation methods to guide which expansions to make and test [32-34]; in the case of the in the case of the kinase active site, however, structural conservation of the hinge-binding motif greatly restricts potential poses of the elaborated compound.

Rather than allow extensive conformational searching, then, we placed each elaborated compound into the kinase active site by alignment of the hinge-binding motif (**Figure 1b**, *Step III*). For each potential elaboration of the hinge-binding motif accessible using the building blocks from the previous step, we generated low-energy conformations using the OMEGA software [35]. Each of these conformers have a shared substructure with the original inhibitor (the hinge-binding motif), allowing them to be individually aligned into the kinase active site (by overlay of the hinge-binding motif, using RDKit [29]). Each protein-ligand complex was subjected to energy minimization using the Rosetta scoring function [36,37], and the lowest-energy conformer that included the expected hinge-binding hydrogen bond pattern was carried forward.

Step IV: Fragment merging

Having separately optimized individual substituents in conjunction with the hinge-binding motif, our next goal was to combine these into a single chemical entity. This task is encountered elsewhere in a separate class of fragment-based drug discovery, fragment merging. Broadly speaking, merging can be used when two different fragments both include a shared functional group that engages the protein the same way, but the two have substituents at different positions; in this case the substituents from each of the two fragments can be joined onto the shared core, and the substituents' interactions with the protein can be preserved [15,16].

By construction, our protocol brings us to the point of having variations on a shared core (the hinge-binding motif) with substituents at different positions. Importantly, though, these can only be reasonably merged if the shared core occupies precisely the same pose in both fragments. Conversely, if either substituent makes interactions with the protein that require changes to the positioning of the shared core, they are fundamentally incompatible with one another, and cannot be merged.

For each fragment elaborating the hinge-binding motif at a given position, we therefore consider whether it can be merged with any of the fragments elaborating the hinge-binding motif at a different position. To determine their compatibility, we evaluate the RMSD for the shared core (the hinge-binding motif) between the two poses: if the RMSD is below a defined threshold, the fragments are merged to yield a new candidate kinase inhibitor (**Figure 1b**, *Step IV*). All potential pairs are exhaustively considered, and thus the effective chemical space spanned by this approach can be very large.

This fragment merging approach also naturally provides the expected pose for this new inhibitor, by simply retaining the coordinates of the shared core, and concatenating together the substituents' coordinates from the corresponding fragments. Importantly, since this fragment merging approach combines the structures of substituents in each one's preferred geometry, one might assume additivity of their interactions. This implies that the interaction energy of the newly-constructed compound with the kinase can be estimated from the interaction energies of the component fragments. This will be explored further using the real examples to follow, but the assumption of energetic additivity between substituents

allows the top-scoring compounds to be identified at this merging stage, without the need to explicitly refine all models.

Step V: Selecting top-scoring inhibitors

Finally, we re-refine and re-score the top-scoring compounds from the preceding step, by energy minimization using Rosetta [36,37] (**Figure 1b**, *Step V*). This step serves to ensure that the selected substituents on the shared hinge-binding core are indeed compatible with one another, both structurally and energetically. Slight differences in the orientation of the shared core can lead to slight deviations from additivity for the substituents, and thus refining and re-ranking them explicitly ensures that the top-scoring new candidate inhibitors are advanced.

Results

To evaluate this protocol, we selected five diverse kinase inhibitors as starting points. Each of the five compounds bears a clear hinge-binding motif, as confirmed through crystal structures in complex with each inhibitor's target kinase (**Figure 2**). However, all five hinge-binding cores are different from one another. Each of the five compounds inhibit their target kinase with IC_{50} better than 20 nM, through the culmination of a medicinal chemistry campaign described in each of the studies reporting these compounds. For clarity we will refer to each of these inhibitors by their names in PubChem. The five inhibitors are:

1) MC180295, a selective CDK9 inhibitor built on a diaminothiazole core [38,39] (PDB ID 6W9E)
2) BDBM50091276, a CHK1 inhibitor built on a 1,7-diazacarbazole core [40] ("compound 8" in the original paper, PDB ID 4RVK)
3) CHIR-124, a CHK1 inhibitor built on a quinolinone core [41] ("compound 11" in the original paper, PDB ID 2GDO)

4) BDBM7773, a CDK2 inhibitor built on an oxindole core [42] ("compound 109" in the original paper, PDB ID 1KE7)

5) BDBM50246162, an ACK1 (aka TNK2) inhibitor built on a pyrazolopyrimidine-3,6-diamine core [43] ("compound 2" in the original paper, PDB ID 3EQR)

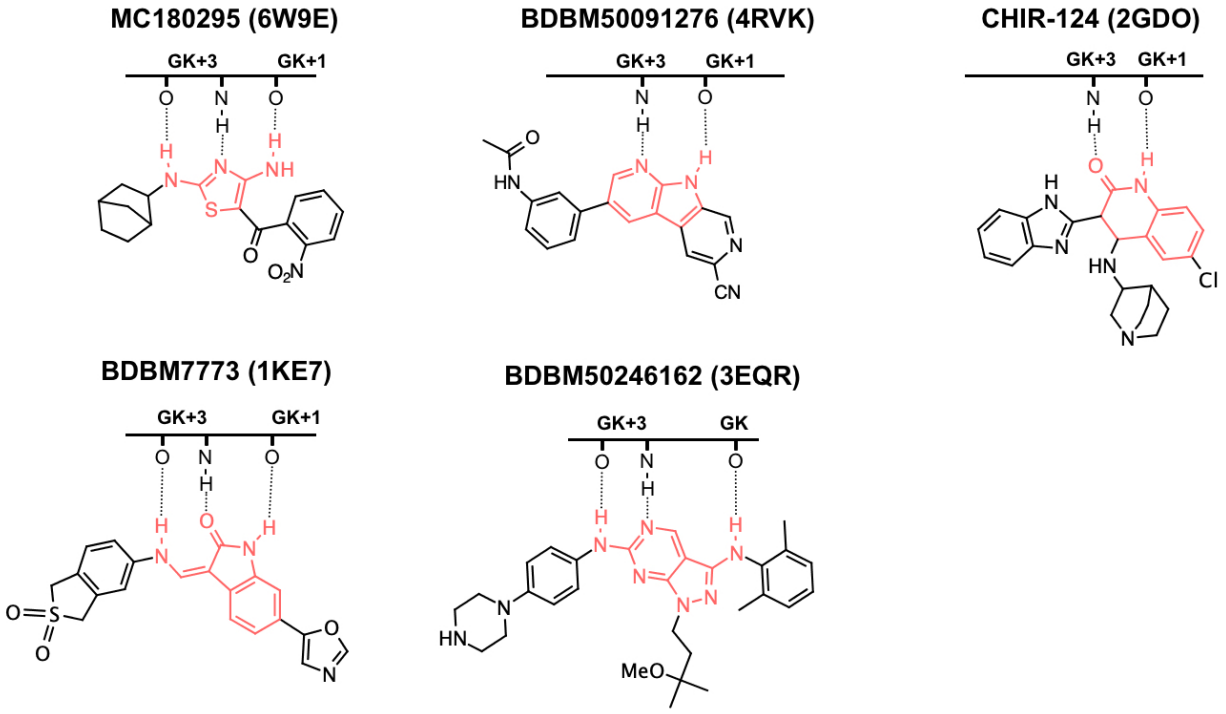

Figure 2: The five kinase inhibitors used as starting points for our study. Each of the kinase inhibitors used as starting point for our study have a clear hinge-binding motif (*red*). The kinase hinge region is represented schematically, with numbering relative to the gatekeeper (GK) residue. The pattern of hydrogen bonds between each inhibitor and the kinase hinge presented here is drawn from the crystal structures of each complex (PDB IDs are provided for each complex). Each of these inhibitors engages the kinase hinge via two or three hydrogen bonds to the GK+1 and GK+3 positions. Inhibitor BCBM50246162 also includes a hydrogen bond to the sidechain of the GK residue (threonine).

In the case of CHIR-124, the crystal structure of this compound in complex with CHK1 shows that its quinuclidine group points directly away from the hinge (**Figure 2**). This large substituent makes somewhat unusual contacts to both the P-loop and the catalytic loop of the kinase, bridging the kinase's N- and C-lobes [41]. We discovered that varying the substituent at this position led to dramatic differences in

the kinase conformation of our models, making it difficult to draw reliable conclusion about the effect of these substitutions. For the purposes of our study, we therefore elected to remove the aminoquinuclidine group from this compound.

Library building from generalized reaction schemes

For each of the five inhibitors to be considered, we used as a starting point the synthetic scheme used to the prepare each compound. As noted earlier, computational methods for synthetic route planning could be used for this step; however, re-using the reported path makes it more likely that analogs reported in each campaign will also be present in our computational library, facilitating benchmarking for this study.

As is typical for preparation of kinase inhibitors, the synthetic schemes are designed to elaborate a particular hinge-binding core with many diverse substituents. The building blocks that contribute groups outside the core are ideally used late in the synthetic route, so that common intermediates may be re-used.

Using the approach described earlier, we generalized each reaction and searched for building blocks matching the patterns required for each chemical transformation. The libraries resulting from enumeration of commercially-available building blocks are, unsurprisingly, astoundingly large (**Figure 3**). In generalizing the synthetic route used to access MC180295, for example, our search revealed about 5,000 2-bromoacetophenones, and 750,000 primary amines: enumerating all pairs leads to almost 4 *billion* diaminothiazoles that could be accessed using this synthetic route. In fact, many more potential inhibitors can be reached though this path, through the trivial synthesis of additional 2-bromoacetophenone building blocks; for this first study, though, we limit our search to the lower bound of libraries that can be immediately accessed using available starting materials.

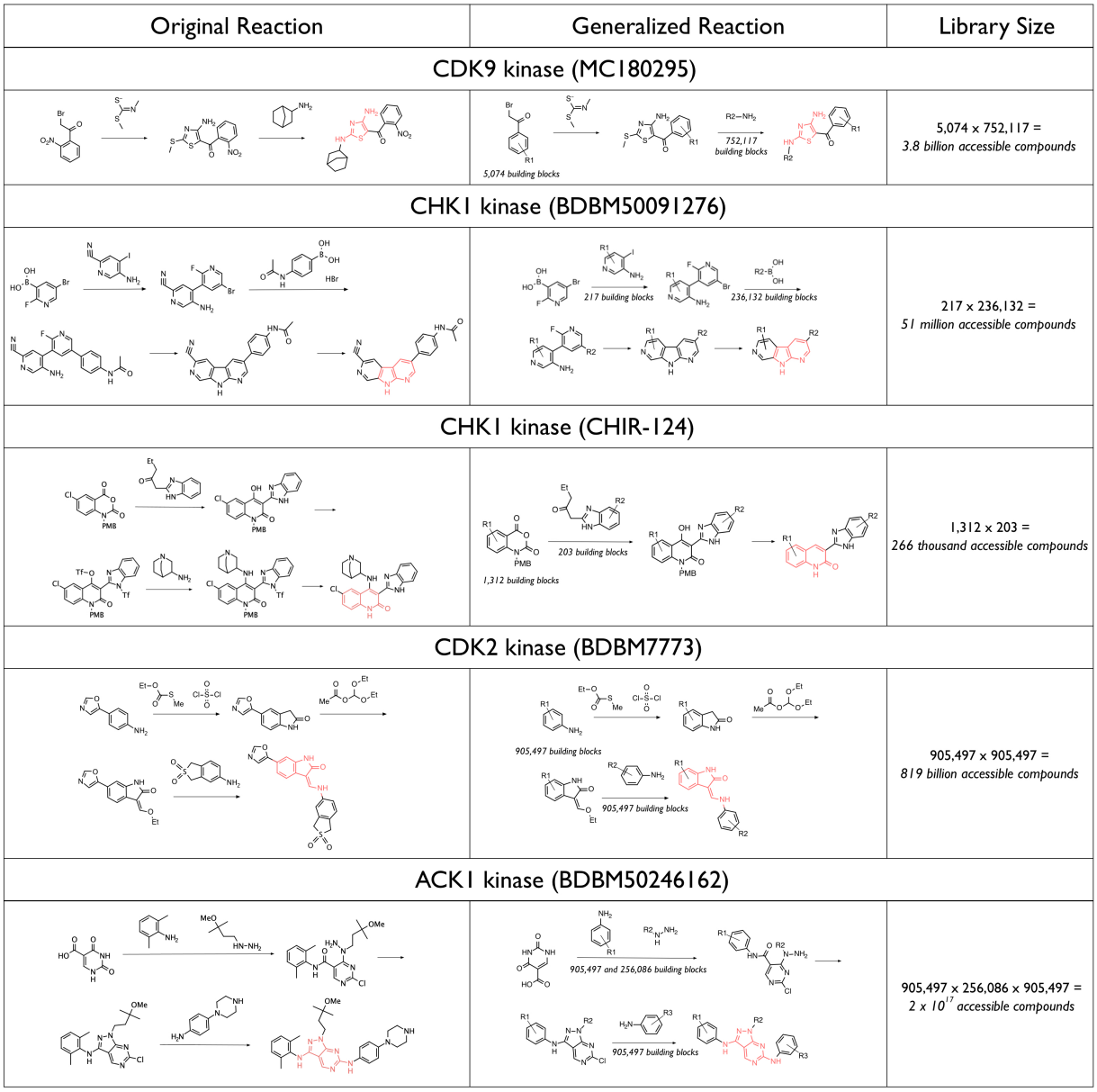

Figure 3: Library building from generalized reaction schemes. *Left column:* The reported synthetic routes for the five representative kinase inhibitors are shown, with the hinge-binding core highlighted in *red*. *Middle column:* Generalizing each reaction by allowing for commercially-available building blocks with diversified substituents enables generation of new compounds that can be accessed through the same synthetic route. *Right column:* Enumerating the chemical space accessible through this strategy demonstrates the magnitude of libraries compiled in this manner.

As expected, the number of available building blocks at each stage is determined by complexity and popularity of the template: generic primary amines, boronic acids, and arylamine (found in the generalized syntheses of MC180295, BDBM50091276, and BDBM7773 respectively) yield many

hundreds of thousands of matching building blocks. By contrast, more specific patterns or those that correspond to obscure starting materials may yield only hundreds of potential alternatives. Naturally, the number of building blocks available for diversification also strongly influences the resulting library size: in the case of BDBM50246162, appending three different substituents from readily-available building blocks results in a much larger chemical space in which to search (2×10^{17} compounds).

For each reaction, we first searched the newly-generated compounds to determine whether the known inhibitor was present in the enumerated library. Essentially, this test simply evaluates whether the required building blocks for this compound were identified from PubChem: in all five cases, this was confirmed to be the case. Moreover, each library also included many of the analogs described by the original authors of each study, allowing for further benchmarking.

Assembling models of bound inhibitors from fragments

Before testing our fragment-based computational approach in a screening context (**Figure 1b**), we first sought to examine whether building up the structure of the known inhibitor from fragments would yield the correct (experimentally determined) pose. For each of the five case studies, we therefore began by applying our computational approach using the fragments that yield the known inhibitor.

As described earlier, low-energy conformers are built from each fragment. Each conformer is then separately aligned into the kinase active site using the hinge-binding motif, subjected to energy minimization, and the fragment with the best interaction energy is carried forward (**Figure 1b**, *Step III*). Using fragments from each of the known inhibitors, we found in all cases that the elaborated functional group adopted a conformation very similar to that observed in the crystal structure of the full inhibitor (**Figure 4a**). Further, we were gratified to see in all cases that the resulting poses retained the intended hinge-binding motif in the appropriate conformation: should either pose position this core in an alternate position, it would not be possible to merge the two fragments.

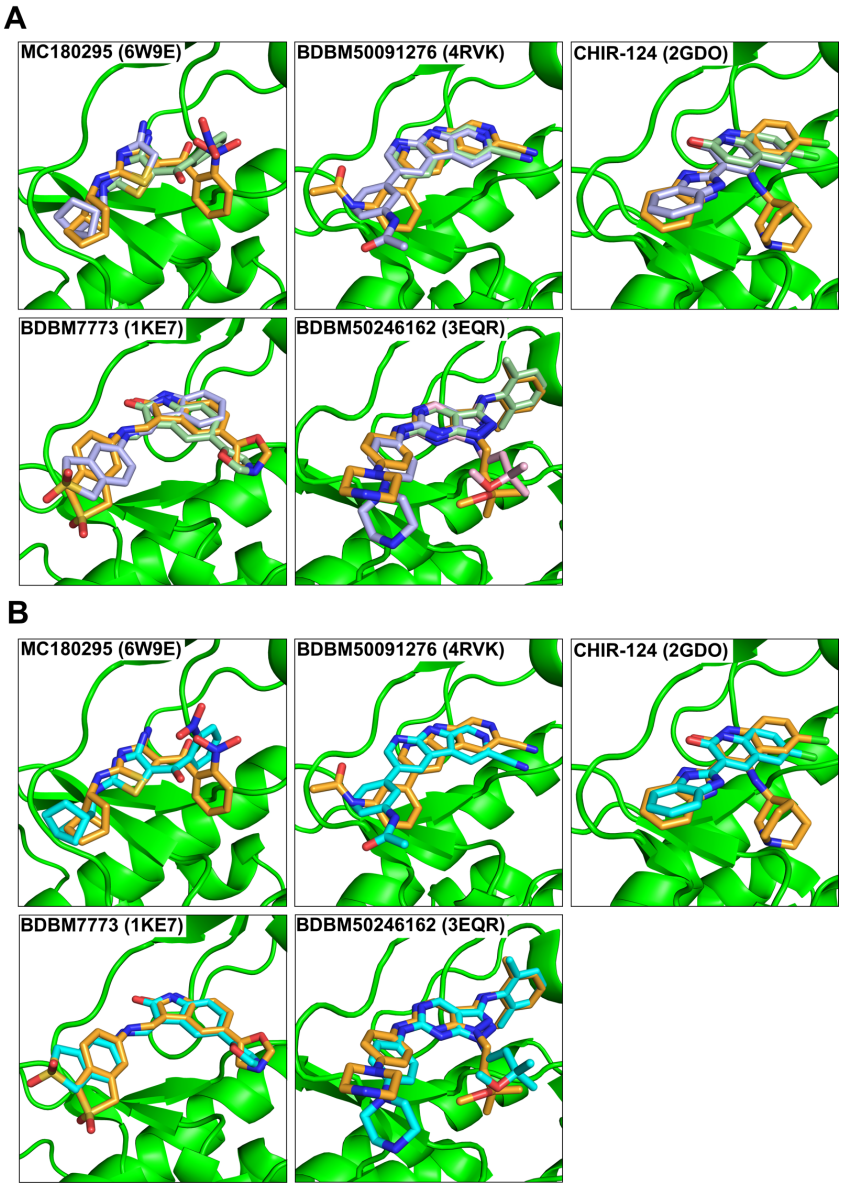

Figure 4: Recapitulation of binding mode for known inhibitors. (**A**) For each of the five known inhibitors, we began from fragments corresponding to the substituents in the known inhibitor (i.e., each fragment comprises the hinge-binding core and one of its side chains). Models were prepared for each fragment in complex with the cognate kinase, and refined via energy minimization. The resulting models of the fragments (*slate and light green*) position the side chains in close agreement with their positions in the crystal structure of the complete inhibitor (*orange*). Moreover, the positioning of the hinge-binding core in both fragments is closely overlaid, allowing the fragments to be merge. (**B**) Merging the fragments and refining the resulting model by energy minimization led to models of the complete inhibitor (*cyan*) that closely match the crystal structures of these compounds (*orange*). As noted elsewhere, throughout this study we have elected to model CHIR-124 without its aminoquinuclidine group (bottom right in this view). This group makes simultaneous interactions to the kinase's P-loop and catalytic loop that bridge the kinase lobes: varying this substituent leads to dramatic differences in the kinase conformation, making differences in interaction energies unreliable.

This was an important and reassuring result, because it implies that – at least for these potent and well-optimized inhibitors – there is no "tug-of-war" between the two sides of the inhibitor. Rather, the individual contributions of the substituents added to the central core are also locally optimal, because their interactions with the protein are the same irrespective of whether other substituents are present on this core.

We then merged each of the cognate fragment pairings (**Figure 1b**, *Step IV*), and re-minimized this model of the full inhibitor (**Figure 1b**, *Step V*). Unsurprisingly, given that the initial model had been built from complementary fragments with a closely shared core, minimization of the complete inhibitor did not result in drastic changes to the pose. Moreover, since the fragments were already in good agreement with the corresponding parts of the inhibitors' crystal structures, the resulting models of the complete inhibitors also closely matched the corresponding experimentally determined structures (**Figure 4b**).

Pairwise additivity of interaction energies

When extending this fragment-merging strategy to a screening context, our intention is to locally optimize the component fragments (**Figure 1b**, *Step III*), then merge them only if the shared core aligns in both cases. A fragment that shifts the positioning of the shared core relative to the starting orientation might be used in an inhibitor, but it can only be credibly merged with another fragment that also shifts the shared core in precisely the same way.

A consequence of merging fragments with structurally-shared cores is that their interactions with the kinase are expected to be energetically additive. Non-additivity between pairs of chemical substitutions can arise for a number of reasons: primarily if the preferred conformation for the two substituents clash with one another, or each requires the protein to adapt in a way that is inconsistent with the other, or due to changes in solvent structure, or if they lead to mutually-incompatible conformation of their shared cores [44-47]. In each of our testcases, substituents are added at vectors pointing in opposing directions, making it unlikely that the substituent at one position (or its effect on the kinase conformation) would be felt at the other position. Individual water molecules are not explicitly modeled in our energy function, eliminating this potential source of non-additivity. Thus, we hypothesized that the interaction energy of the kinase

inhibitors comprising our libraries could be predicted from the energies from the fragments, provided that the location of the shared core is the same in both fragments.

To test this hypothesis, we sought to evaluate the expected interaction for a full inhibitor from its fragments (given the assumption of pairwise additivity), and then explicitly assembled this inhibitor and explicitly evaluate its interaction energy (after minimization of the full inhibitor). Because this experiment requires explicit minimization of each candidate inhibitor, it cannot be carried out to completion using the huge libraries of accessible compounds described earlier (**Figure 3**). Instead, we randomly selected a subset of fragments for each building block, and exhaustively enumerated smaller libraries of accessible compounds (typically several hundred thousand compounds) (**Figure S1**).

Original Reaction	Generalized Reaction	Library Size
CDK9 kinase (MC180295)		
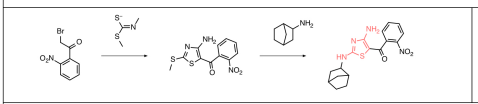	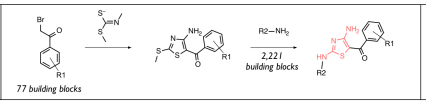	77 x 2,221 = *171,017 accessible compounds*
CHK1 kinase (BDBM50091276)		
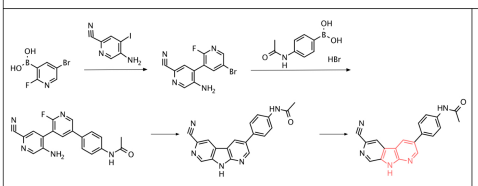	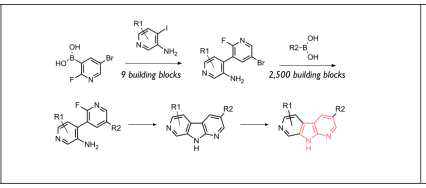	9 x 2,500 = *22,500 accessible compounds*
CHK1 kinase (CHIR-124)		
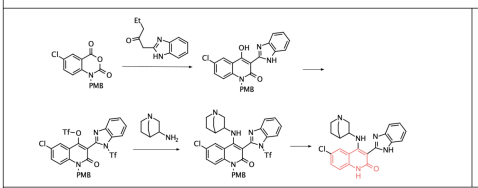	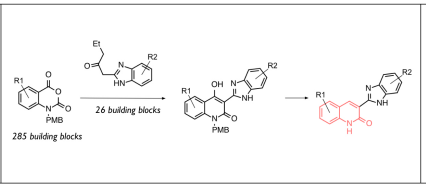	285 x 26 = *7,410 accessible compounds*
CDK2 kinase (BDBM7773)		
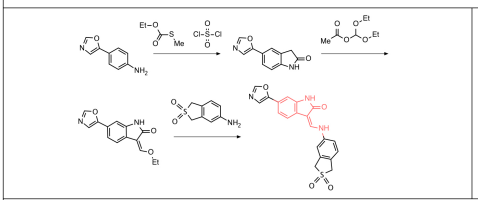	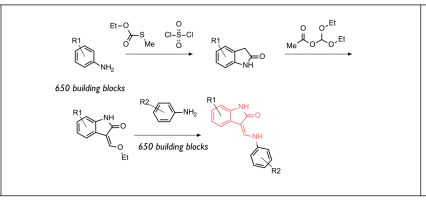	650 x 650 = *422,500 accessible compounds*
ACK1 kinase (BDBM50246162)		
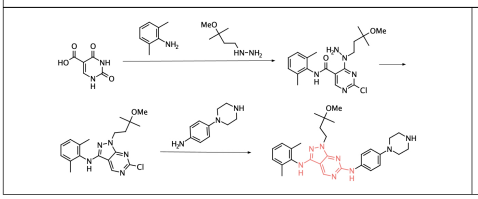	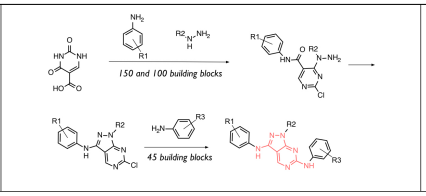	150 x 100 x 45 = *675,000 accessible compounds*

Figure S1: Smaller libraries for evaluating pairwise additivity approximation. Determining the appropriateness of the pairwise additivity approximation requires explicitly evaluating compounds' interaction energies in a non-pairwise way; this precludes the use of huge chemical libraries. For this experiment we therefore selected randomly a subset of the building blocks for each reaction. Enumerating these reactions now provides much smaller chemical libraries that can be explicitly screened.

We built models corresponding to each of the fragments in this library as described earlier (**Figure 1b**, *Step III*), minimized them in complex with the kinase, and determined their interaction energies. Based on a standard chemical double-mutant cycle [48] (**Figure 5a**), albeit here using interaction energies from Rosetta rather than true binding free energies, we evaluated the interaction energy expected for each compound in our library. We then merged each of the cognate fragment pairings (**Figure 1b**, *Step IV*), and minimized this model of the full inhibitor (**Figure 1b**, *Step V*).

Results from this experiment show that for our first four testcases, the interaction energy estimated with the pairwise approximation closely matches the full inhibitor's interaction energy calculated explicitly (**Figure 5b**), as observed through points that lie along the diagonal of these plots. Agreement between the two values is highest when the position of the core scaffold matches very closely among the two fragments, as expected. For the BDBM7773 library, some of the compounds have with worse interaction energy than expected based on additivity (points below the diagonal); however, these the points have relatively high RMSD (dark green rather than light green). Put another way, merged compounds with worse interaction energies than expected from the pairwise approximation occur when the fragments do not position the shared core in precisely the same location.

This observation is especially acute for the BDBM50246162 library: since this library diversifies three positions rather than just two, very few fragment triplets place the core in precisely the same position. Very few groupings of fragments in this library have low RMSD (i.e., it is unlikely to find all three that position the core in precisely the same way), and thus many of the merged inhibitors lie below the diagonal. As a consequence, this observation implies that it will be necessary to consider huge libraries when three positions are diversified, if one seeks to find mutually compatible combinations of fragments.

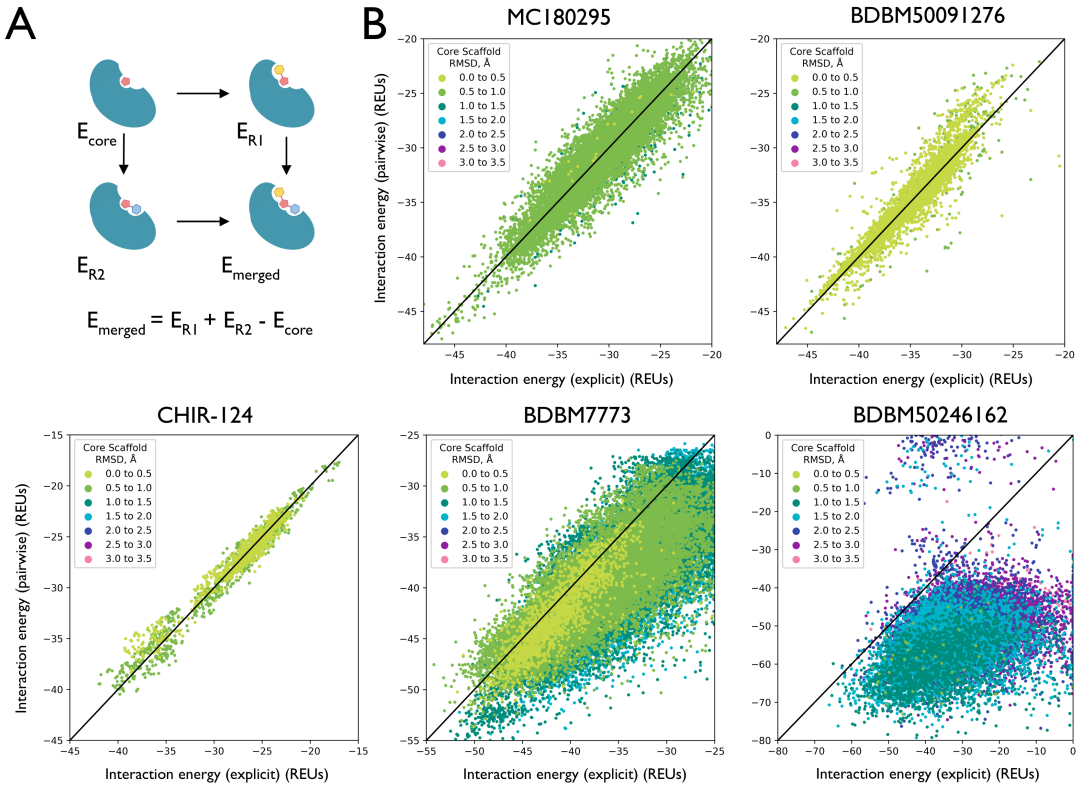

Figure 5: Pairwise additivity allows the inhibitors' interaction energies to be predicted from their component fragments. (**A**) Chemical double-mutant cycle for estimating the merged inhibitors' interaction energy. Subject to the pairwise additivity approximation, the interaction energy of the merged compound (E_{merged}) is given by the sum of the fragments' interaction energies (E_{R1}, E_{R2}) minus the interaction energy of the hinge-binding core (E_{core}) which is present in both fragments. (**B**) Interaction energies are reported for each compound in the five libraries, either estimated from the component fragments using the pairwise approximation (y-axis), or calculated explicitly from the re-refined model of the complete inhibitor (x-axis). Energies match closely (*points along the diagonal*) provided that the RMSD is small between the fragments' positioning of their shared core (*light green points*). As the RMSD becomes larger (*blue and purple points*), the interaction energy of the complete inhibitor is often not as favorable as expected from the pairwise approximation (*points below the diagonal*). Interaction energies are reported in Rosetta energy units (REUs).

Beyond binding affinity, of course, kinase inhibitor selectivity is paramount in hit-to-lead optimization. To explore whether the same pairwise approximation could be used to evaluate selectivity, we built models for all 171,017 compounds in the MC180295 library in complex with ten different CDK kinases. For each model, we evaluated the energy assuming pairwise additivity (from the component fragments), and then separately re-minimized the complex and evaluated the compound's interaction energy

explicitly. Using these explicitly-calculated interaction energies, we then identified the preferred kinase for each compound.

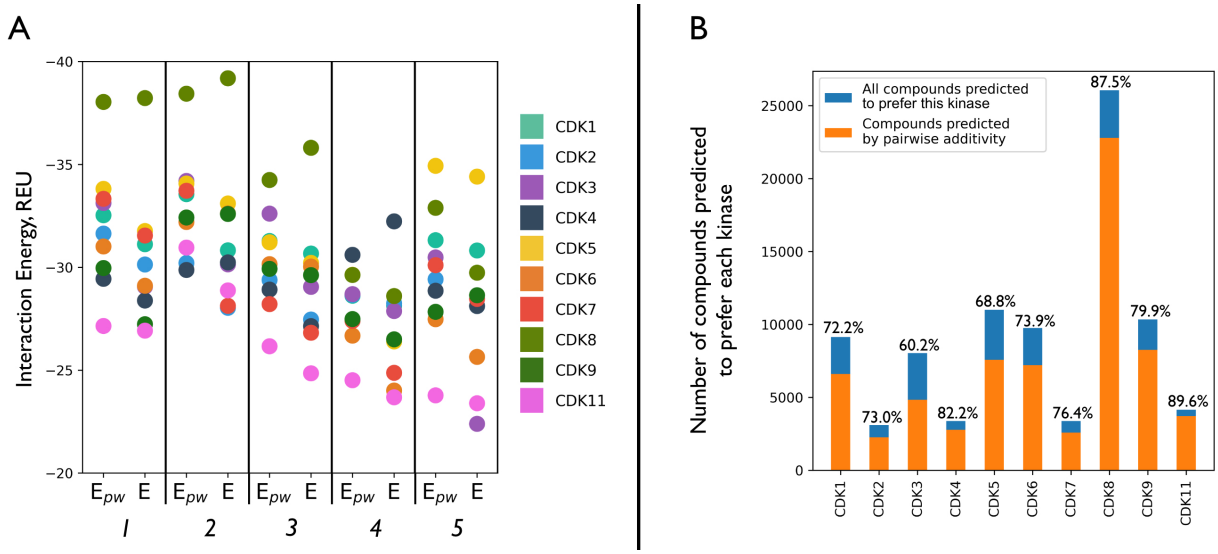

Figure 6: Selectivity can also be recapitulated using pairwise additivity. For each compound in the MC180295-inspired library, we build models in complex with 10 members of the cyclin-dependent kinase (CDK) family. Interaction energies were estimated from the component fragments using the pairwise approximation, and also calculated explicitly from the re-refined model of the complete inhibitor. (**A**) Interaction energies for five different compounds in this library (1-5), as calculated with or without the pairwise approximation. For all five compounds the preferred kinase is correctly identified, but the magnitude of the energy gap (relative to the next kinase) is not always accurately recapitulated. Interaction energies are reported in Rosetta energy units (REUs). (**B**) For the compounds in the library that prefer a given kinase (based on their explicitly-calculated interaction energies), the preferred kinase was correctly assigned using the pairwise approximation 78% of the time. The number of compounds in our library preferring each of these 10 CDK kinases was not uniform: these chemical scaffolds exhibited a preference for CDK8 over the other family members. Nonetheless, the pairwise approximation proved similarly effective for all ten kinases at selecting the compounds that preferred the kinase of interest.

In many cases, the explicitly calculated CDK-family preference of individual compounds was well-recapitulated by the pairwise approximation. Drawing from five representative compounds (**Figure 6a**), we observe that in some cases the less favorable pairings are not always accurately predicted; however, these less favorable pairings are not relevant for determining a compound's preferred kinase.

Overall, 88,364 compounds could be assembled from fragments that maintained the expected hydrogen bonding to the kinase hinge, and also positioned the hinge with low RMSD among the fragments (i.e., allowing the fragments to be merged). The distribution of kinase preference for these compounds was

far from uniform: many were predicted to prefer CDK8 over the other CDK family members, and compounds predicted to be selective for CDK2, CDK7, and CDK11 were relatively rare. Somewhat surprisingly, the preferred kinase for an individual compound could be ascertained 78% of the time using the pairwise estimates of their energies (**Figure 6b**). Of the 26,053 compounds designated CDK8 inhibitors based on their explicitly-calculated interaction energies, for example, 22,793 of these had also been designated as CDK8 inhibitors using their pairwise energies (87.5%). Given that there were 10 kinase included in this study, one would expect to correctly assign the preferred kinase by chance only 10% of the time.

This observation suggests that it may be possible to quickly assign the expected selectivity of compounds in a huge library using the pairwise approximation, and then carry forward for explicit refinement only those inhibitors which are predicted at this stage to be selective for one's kinase of interest.

Screening huge chemical libraries

It is important that the calculated interaction energies of kinase inhibitors can be reliably estimated from the interaction energies of its component fragments (provided that the cores are well-aligned with one another), because this implies that the original (huge) enumerated libraries need not be screened explicitly. Rather than build models for each compound in complex with the target kinase, one can instead build models only for the component *fragments*, and from these infer the interaction energies of the complete compounds. From a screening standpoint, one can thus identify the top-scoring compounds from these huge libraries extremely rapidly, and use the prescribed synthetic route to make several compounds and test their activity.

While experimentally validating the top-scoring compounds lies beyond the scope of this first study, we note that the five inhibitors that inspired our study were themselves the culmination of campaigns that re-used the same synthetic route to explore many analogs. From the publications describing these inhibitors [39-43], we therefore selected the four most potent analogs reported in each study, and asked

whether our method would prioritize these compounds from among the vast swath of enumerated chemical space.

We began by confirmed that the fragments needed to build each of these analogs were present in our enumerated libraries. For convenience, we then restricted the size of each fragment collection to 10,000 (while preserving those needed for building the reported analogs), simply to avoid having to screen nearly a million building blocks in some cases (**Figure 3**). We then further filtered the fragment sets to remove large substituents (that would bring the final inhibitors molecular weight over 500 Da) and atom types not supported by the OMEGA software. For each library, we then built models corresponding to all fragments bound to the cognate kinase, and evaluated their interaction energies. Using this pairwise additive approximation, this fast calculation allows estimation of the interaction energy for all compounds in these huge libraries.

To reiterate the effect of the pairwise additive approximate on the computational demands of these screen, we use as a representative example our screen of the MC180295 library. For each fragment, up to 10 conformers are separately minimized in complex with the kinase (the degrees of freedom are restricted to the substituent, making a small number of conformers is sufficient). A total of 2914 fragments were considered for the first substituent (29012 conformers), and 9399 fragments (90085 conformers) for the second substituent. Each conformer was minimized in complex with CDK9, for a total of 119,097 independent minimizations. These took an average of 2.5 min on relatively slow CPU's, for a total of 4962 CPU-hours. By running these calculations on a typical cluster, the complete set of fragment interaction energies can thus be collected in a matter of hours (elapsed real time, aka "wall time"). Using this modest calculation, we can then infer interaction energies for all 27 million compounds (2914 x 9399) that comprise our enumerated library. While fast docking methods have been used to screen even larger libraries than this [7], these have required vastly larger computational resources and have screened against a fixed protein conformation: by contrast, the minimization step used here allows the protein to adjust its conformation in response to different ligands.

The interaction energy calculated using Rosetta [36,37] comprises a sum over pairs of atoms, and consequently tends to strongly favor larger ligands over small ones (by virtue of having more atoms, large ligands simply accumulate more interactions). The same trend broadly holds for experimentally-measured binding affinities as well (larger compounds tend to have better potency), which is problematic because larger compounds may be less advanceable due to future PK problems; accordingly, many optimization campaigns instead prioritize compounds on the basis of "ligand efficiency" (binding free energy divided by the number of non-hydrogen atoms) or related metrics [49-51]. To align with these goals, we ranked compounds in our enumerated screening libraries on the basis of their substituents' calculated ligand efficiency (Rosetta interaction energy divided by the number of non-hydrogen atoms).

We present the relative ranking of the known analogs relative to the rest of the enumerated libraries using receiver operating characteristic (ROC) curves. For each model system, this provides a means to present the fraction of the library that ranks ahead of the each of the five analogs known to the active against the kinase of interest. While this is a standard approach for presenting retrieval of known active compounds in virtual screening benchmarks, though, it is not without well-understood biases [52-56]. Specifically, this analysis assumes that all "decoy" compounds (the compounds in the library not designated as "actives") are inactive; thus, a good method should prioritize the known actives ahead of all the decoy compounds. If the decoys are clearly absurd with regards to their complementary for the protein target, they can be easily discarded and any method will appear to have excellent performance; thus, the difficulty of a given benchmark depends on the extent to which the decoys are suitably reasonable for the protein target and/or property-matched to the actives. With respect to suitably matched decoys, however, it is important to note that the "decoys" are typically compounds that have not even been tested for the activity of interest. If the likelihood of a decoy compound having activity is low, then the assumption that they are truly inactive may hold. On the other hand, if the decoy compounds are similar enough to the active compounds, they may themselves also have activity; these could then be (correctly) prioritized by the screening method, but penalized for doing so (because all decoys are assumed to be inactive).

In our experiment, the enumerated libraries bear the same core scaffold as the known actives, and many substituents have size and chemistry that is likely to make these active as well. For this reason, many of the decoy compounds in this experiment are themselves likely active; even a method providing "perfect" performance would not distinguish the five actives that happen to have been experimentally characterized versus the undiscovered actives in our library. Thus, the layout of this experiment is such that a very conservative perspective of performance will be conveyed.

As a starting point, we first carried out this screen using the structure of the kinase that had been solved in complex with one of the reported inhibitors (**Figure 7**, *blue*). For all five cases, the known analogs were retrieved far sooner than would be expected by random chance (**Figure 7**, *green*). By random chance, one would expect to need a subset comprising 20% of the original library to find one of the five analogs; in contrast, for all but one of these libraries a collection of the top-scoring 1% of compounds contains at least one of the known actives (MC180295 is the only exception).

These first screens were carried out starting from a kinase crystal structure that was determined in complex with an inhibitor bearing the same hinge-binding motif as all compounds in the enumerated library. While structures of related compounds are likely to be available in a true hit-to-lead scenario, we nonetheless sought to examine performance when such a structure is not available. Accordingly, we carried out the same screens starting from nucleotide-bound crystal structures of the same kinases. We find that performance is only slightly diminished in this regime (**Figure 7**, *orange*), with one exception: for the CHIR-124 library, the fragments needed to build the reported analogs do not yield hinge-binding poses, and are thus not found in our screen.

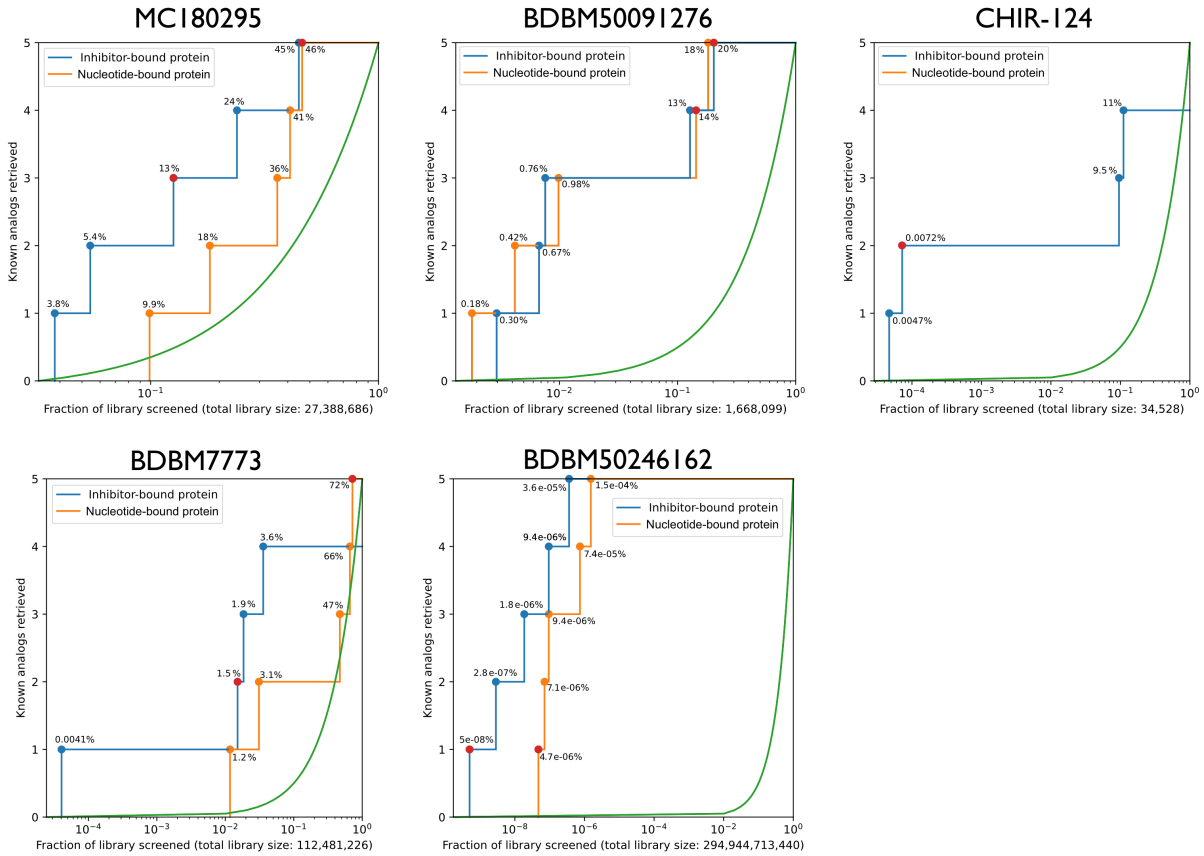

Figure 7: Large-scale screening of enumerated libraries using the pairwise additive approximation. For each of the five inhibitors in our set, we built enumerated libraries and ranked the compounds on the basis of their substituents' ligand efficiency (thus, scores arose in a pairwise additive way). Each library included five analogs reported to have activity against the target kinase. We plot the fraction of the library that must be screened before encountering each of these five active compounds (noting that many of the compounds ranked ahead of these five compounds may themselves also be active). In all five cases, the compounds reported in the literature to have activity are ranked more favorably within the library than expected by chance (*green curve*). Of the five analogs, one of them (*red dot*) corresponded to the inhibitor present in the crystal structure from which the kinase conformation was taken (*blue curve*). Screening was separately carried out using a kinase conformation that was instead solved in complex with a nucleotide (various ATP analogs) (*orange curve*). The size of these libraries ranged from 34 thousand up to 295 billion compounds; by assuming pairwise additivity, these could be screened in a matter of hours on a typical cluster while including protein flexibility in response to the various substituents.

We also sought to understand whether starting from a crystal structure solved in complex with one particular inhibitor would bias the screen to "rediscover" the compound used in solving the structure: if so, this would inadvertently focus hit-to-lead exploration of chemical space near the known structure. To test this, we evaluated the order in which the five analogs were ranks: in all but one case, the compound used

for crystallography was *not* the top-scoring amongst the five known analogs (**Figure 7**, *red dot*), confirming that our modeling protocol allows sufficient flexibility for the kinase structure to accommodate alternate substituents.

The chemical structures of the analogs themselves further highlight the ability of this approach to recognize active compounds with diverse substituents (**Tables 1-5**). However, the redundancy that is evident among the analogs for a given target (the same R1 substituent is used with multiple R2's, and vice versa) also serves as a reminder that many more combinations of these substituents are also likely to be active, if they can be combined using a shared positioning of the hinge-binding core. Because these compounds would not be designated as "active" in our ROC plots, the true performance of this approach is likely superior to that suggested by this retrospective analysis. Simply put, the chemical space available by enumerating these reactions is far larger than can be explored via "wet" medicinal chemistry.

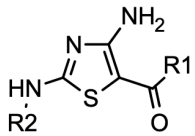

Compound name	R1	R2	Rank, %
MC180340	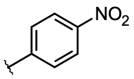		3.8
MC180343	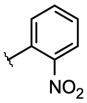		5.4
MC180295	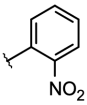		12.6
MC180349	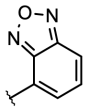		23.9
MC180342	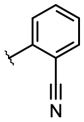		44.7

Table 1: Analogs of MC180295 previously reported to have activity against CDK9 [39]. The rank of each analog in our screen is provided relative to the complete enumerated library (**Figure 7**). The compound present in the crystal structure (i.e., MC180295 itself) is indicated in *red*.

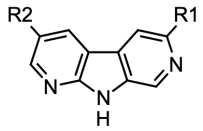

Compound name	R1	R2	Rank, %
C45	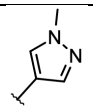	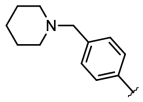	0.3
C41		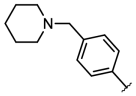	0.7
C46		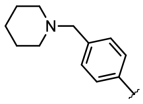	0.8
C34		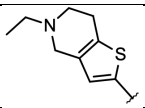	12.8
C8		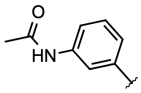	20.3

Table 2: Analogs of BDBM50091276 previously reported to have activity against CHK1 [40]. The rank of each analog in our screen is provided relative to the complete enumerated library (**Figure 7**). The compound present in the crystal structure (i.e., BDBM50091276 itself) is indicated in *red*.

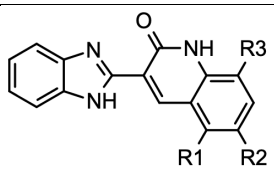

Compound name	R1	R2	R3	Rank, %
C6*	H	CH3	H	0.0047
C9*	H	Cl	H	0.0072

C14*	Cl	Cl	H	9.55
C4*	H	H	H	11.1
C15*	H	H	CH3	N/A

Table 3: Analogs of CHIR-124 previously reported to have activity against CHK1 [41]. The rank of each analog in our screen is provided relative to the complete enumerated library (**Figure 7**). The compound present in the crystal structure (i.e., CHIR-124 itself) is indicated in *red*. The final compound presented was not ranked in our screen, because the corresponding fragment did not retain the required hydrogen bonds to the kinase hinge region.

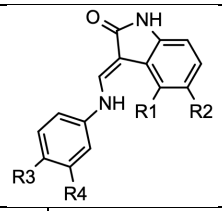

Compound name	R1	R2	R3	R4	Rank, %
C55	H	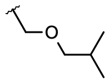		H	0.0041
C109	H	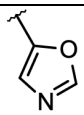	-CH2-S(=O)(=O)-CH2-		1.5
C23	H	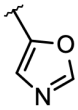		H	1.9
C53	H			H	3.6
C82	=CH-CH=CH-N=			H	77.4

Table 4: Analogs of BDBM7773 previously reported to have activity against CDK2 [42]. The rank of each analog in our screen is provided relative to the complete enumerated library (**Figure 7**). The compound present in the crystal structure (i.e., BDBM7773 itself) is indicated in *red*.

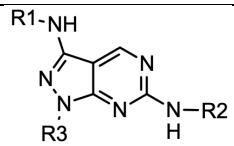

Compound name	R1	R2	R3	Rank, %
C2	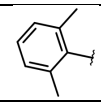	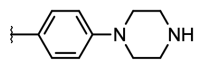	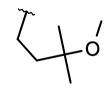	4.9E-10
C13	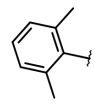	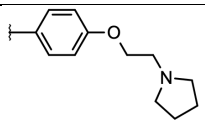	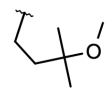	2.8E-9
C12	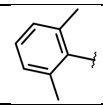	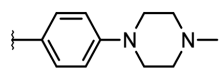	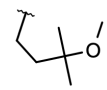	1.9E-8
C14	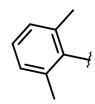	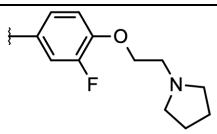	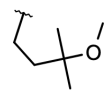	9.4E-8
C11	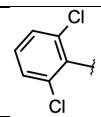	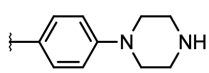	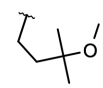	3.6E-7

Table 5: Analogs of BDBM50246162 previously reported to have activity against ACK1 [43]. The rank of each analog in our screen is provided relative to the complete enumerated library (**Figure 7**). The compound present in the crystal structure (i.e., BDBM50246162 itself) is indicated in *red*.

Discussion

In light of the intense focus on kinases as drug targets, there has been extensive interest in streamlining hit-to-lead optimization for this target class – including through computational methods.

With respect to library building, for example, methods have been recently described for deconstructing sets of reported kinase inhibitors, then reassembling these into new collections for screening. One such method operates at the level of chemical structure, by assigning each piece of a known inhibitor to be either a “core” (hinge-binding) fragment, a “connecting” fragment, or a “modifying” fragment. These fragments were then recombined to yield a library of 39 million compounds, albeit with the caveat that the

three-dimensional fit of these compounds with respect to the ATP-binding site has not been established [57]. Addressing this, a complementary method instead elected to divide the ATP-binding site into six sub-pockets, and collect from the PDB each of the various fragments that have been observed to occupy these. The authors then recombine fragments drawn from different structures, to yield a library of nearly 7 million new compounds [58]. In both cases, the resulting libraries are highly enriched in novel chemical matter, but synthetic accessibility of the generated compounds is not assured. By contrast, the libraries that we present here are vastly bigger than these earlier libraries, because we instead enumerate compounds that can be constructed using commercially-available building blocks, rather than simply using pieces of existing kinase inhibitors. While not guaranteed, the likelihood that the compounds in our enumerated libraries will be synthetically facile is also much higher, because each compound is included specifically because it is likely to be amenable to assembly using a pre-determined synthetic route.

Beyond just kinase-focused methods, more general strategies for de novo design of new compounds have been broadly explored for more than 30 years. Whereas early methods proposed for this task often produced compounds for which synthetic tractability was a major limitation [59], a number of more recent approaches have been validated in retrospective and prospective evaluations to confirm both synthetic tractability and activity for the biological target of interest [60]. New methods for growing ligands into a (fixed) protein environment continue to be an active focus of research, particularly using fragment replacement strategies [61], genetic algorithms [62], and deep learning [63]. Modern methods can yield impressive performance, though typically with the caveat that benchmarking typically entails building back a ligand into the protein structure it was taken from – so, it remains unclear if (or how well) these methods can accommodate changes to the protein structure in response to the ligand.

Overall, our library-building strategy is most similar to that encoded as part of the Diversity-Oriented Target-focused Synthesis (DOTS) workflow [64]. This iterative hit-to-lead strategy starts from the crystal structure of an initial fragment hit, and considers chemical transformations (using available building blocks) that could be used to elaborate the fragment. The elaborated fragments are ranked using virtual screening, then the top-scoring compounds are synthesized and tested (using robotic instrumentation

for the synthesis). The top-performing derivatives are then used as the starting point for a new round of optimization. Another related approach, PathFinder [65,66], uses free energy perturbation (FEP) calculations to evaluate synthetically-tractable substituents, coupled with active learning to reduce the computational requirements by inferring effects of substitutions that have not yet been explicitly modeled.

Using enumerated libraries, it is easy to very quickly build up chemical libraries that become too large for explicit virtual screening. This has already been observed in the context of computational hit finding (i.e., naïve screening, as opposed to hit-to-lead optimization), enabled by the growth of "make-on-demand" catalogs from vendors including Enamine [7]. Back when this library comprised "only" 170 million compounds, it was possible to explicitly dock each compound through a massive brute-force campaign [7]. By now, the library has grown to 19 billion compounds available for delivery, which far exceeds what can be addressed through any kind explicit structure-based screening. Our own previous work explicitly screened diverse representatives of an intractably large library to search for useful chemotypes first, then extracted from the library analogs of these compounds for a second round of screening [9]. Other studies have trained machine learning models to predict docking scores from chemical structures, as a means to rapidly obtain the outcomes from docking in a much less resource-intensive way [67,68].

The key finding of our study is that we can quickly and reliably estimate the interaction energy for the compounds in our enumerated libraries, by assuming pairwise additivity of the substituents. This is important, because it allows us to assign energies across huge libraries, without needing to explicitly dock each compound: only the component fragments need to be docked, and the compatibility of their poses verified. With respect to hit-to-lead optimization, it also confirms that one can find the compounds with the best interaction energies by simply selecting the best fragments and merging them with one another – but only if the fragments' shared cores are precisely aligned with one another in the binding site.

Traditional hit-to-lead optimization in medicinal chemistry focuses on building up structure-activity relationships by evaluating the functional consequence of separately changing individual side chains: the underlying hope is that after multiple substituents are separately optimized, they can later be productively merged. Unfortunately, this frequently does not quite turn out to be the case, as the

substituents' contributions are often non-additive [69]. At first, this seems to run counter to the claim we make here, that fragment contributions *are* strongly additive.

A recent study carried out a careful survey of examples from the literature that demonstrate strong and verifiable non-additivity, in a variety of different protein-ligand systems for which crystal structures are available [46]. In nearly every example identified, the authors find that the ligand exhibits an altered binding mode in response to one or more of the substitutions. Thus, the conclusion from these examples aligns closely with our own observation, that additivity can be assumed only if the shared core does not change position. While it is not feasible to use x-ray crystallography to verify the binding modes of all fragments in a hit-to-lead optimization campaign, an inherent advantage of using structure-based modeling for driving SAR is that the binding modes are provided for each fragment. This, in turn, is necessary to inform on which fragments can be productively merged with one another.

In our screens, a relatively high proportion of the fragment cores could be merged with one another. In part, this was due to our decision to focus at the outset on kinase inhibitors: as noted earlier, these inhibitors engage the kinase hinge region in a set of prescribed hydrogen bonds (**Figure 2**). This interaction is very strongly templated, and thus tends to be closely recapitulated amongst the fragments that elaborate the hinge-binding scaffold. Thus, the architecture of the kinase binding site contributes to the conserved pose of the shared core, which in turn leads to additivity of the substituents. Conversely, and in keeping with the survey of examples in which non-additivity is observed [46], we do not expect that the same high proportion of fragments can be merged with one another for binding sites that lack a strongly templated interaction to enforce the pose of the shared core.

While fragment pose prediction has historically proved challenging, improved methodologies have now delivered dramatic successes [70-72]. Looking forward, we expect that continued advances will soon allow for reliable identification of fragments that share overlapping cores. Such fragments can naturally be merged on the basis of their shared core, and then libraries to diversify the component fragments will provide a natural path for hit-to-lead optimization.

Finally, we leave with the caveat that the pairwise additive approximation allows for very rapid screening of huge chemical libraries on the basis of interaction energies. The use of interaction energies fundamentally ignores contributions from binding conformational entropy, and calculations are carried out in the absence of explicit solvent: accordingly, one cannot expect these interaction energies to strictly correlated with the compounds' binding affinities. Much akin to deep learning models for predicting docking scores [67,68], this strategy merely provides a way to rapidly estimate an admittedly-crude quantity (interaction energy) that cannot be evaluated at the scale needed to keep up with the growth of library sizes. It will prove very natural to integrate this strategy into a layered approach, by which the size of the library is progressively culled through the use of increasingly-expensive methods, and ultimately using tools such as free energy perturbation (FEP) calculations [73] and orthogonal machine learning scoring functions [9], in combination with tools for predicting ADME-PK [74], to select compounds for further study.

Methods

Computational protocol

Computational tools to enable the use of this protocol are publicly available on GitHub (https://github.com/karanicolaslab/CombiChem).

For a given fragment, protonation states and tautomeric states were assigned using OpenEye QUACPAC FixpKa, using pH 7.4. Partial charges assigned were in OpenEye's QUACPAC (assigncharges.py, using AM1BCC). Conformers were generated using OpenEye OMEGA. For our analysis of pairwise additivity, we generated up to 100 conformers for each fragment, and used an RMS threshold of 0.6 Å for conformer deduplication. For our screens, we instead generated 10 conformers for each fragment, and used the flags "-fixfile" and "-deleteFixHydrogens false" to keep the hinge-binding core fixed (thus restricting conformational diversity onto the substituent).

Alignments into the protein structure were carried out using RDKit, based on the core hinge-binding motif. Structures were then refined using PyRosetta's MinMover for energy minimization, with the L-BFGS gradient minimizer at a convergence threshold of 1E-0.6, and the interaction energies were reported by PyRosetta.

Structures of the kinase-bound fragments were merged into the complete inhibitor using a Python script (included in the GitHub repository above). Finally, the complete inhibitor (after merging) was re-minimized using the same PyRosetta protocol, and the interaction energies were collected.

Results described in our study were generated using OMEGA version v3.0.0.1, QUACPAC version 2.0.2.2, RDKit version 2020.03.3.0, and PyRosetta version 2020.03.post.dev+57.master.

Steps to ensure pairwise additivity of fragment scores

Our initial attempts to use the chemical double mutant cycle presented earlier (**Figure 5a**) did not yield strongly pairwise additive interaction energies. Careful decomposition of the contributions to the evaluated energies pointed to four factors that were responsible for essentially all of the non-additivity (**Figure S2**).

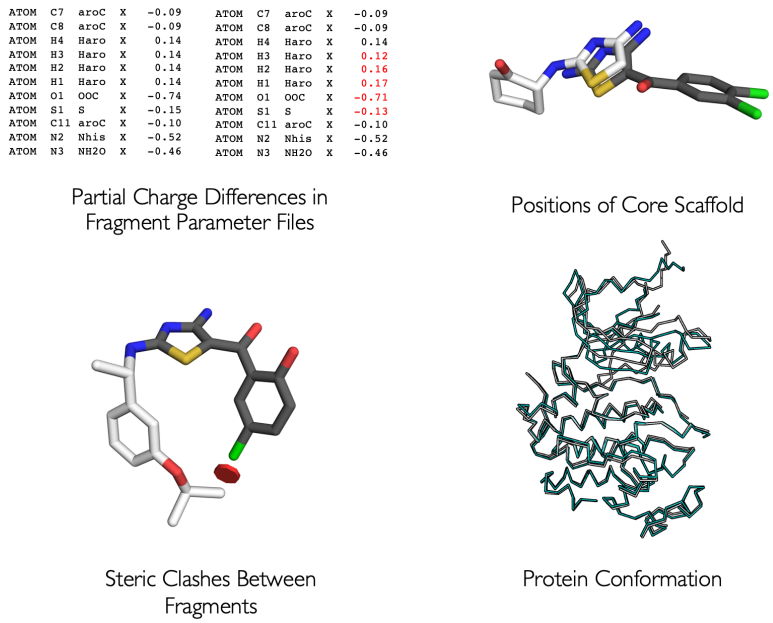

Figure S2: Basis for non-additivity in modeling kinase inhibitors from fragments. Early calculations yield results that were not strongly pairwise-additive, making these unsuitable for estimating interaction energies of the merged compounds. We found that this non-additivity can arise from 1) inconsistent assignment of partial charges, 2) steric clashes between substituents, 3) incompatible positioning of the core hinge-binding motif, or 4) differences in the modeled conformation of the protein in response to different fragments.

To obtain interaction energies that are closely pairwise additive, we found the following steps to be necessary:

1) Consistent parametrization: Partial charges were often assigned differently between the full inhibitor and the corresponding fragments. For this reason, we generated partial charges only using the full inhibitor, then transferred these charges to fragments.
2) Avoiding steric clashes between substituents: Scenarios can arise in which two different fragments present a substituent that occupies the same region of the binding site. When merged, the two substituents obvious clash with one another. For the examples presented in our study, this scenario occurred only in a very small number of cases (involving long and flexible substituents), because the substituted vectors on these hinge-binding cores point away from one another.
3) Positioning of the hinge-binding core: If two substituents each prefer a conformation of the shared core that is inconsistent with the other substituent, then both cannot be satisfied in the context of the merged compound. As presented earlier (**Figure 5b**), this source of non-additivity can be greatly mitigated by merging only pairs of fragments that position the hinge-binding motif in precisely the same pose.
4) Protein conformation: Similarly, if two substituents each require that the protein adopts a conformation that is inconsistent with the other substituent, then both cannot be satisfied in the context of the merged compound. As noted earlier, kinase inhibitors typically have a flat hinge-binding core, with substituents that extend in both directions parallel to the hinge (**Figure 2**). The substituent facing the kinase's αC-helix occupies the so-called "hydrophobic back-pocket" of the binding site [75] (**Figure 2**, *right side of the compounds drawn*), and can be associated

with structural changes in response to the different inhibitors. By contrast, substituents at the other side of the hinge-binding core are typically partially exposed. Thus, modeling fragments that face the αC-helix often lead to small structural changes, whereas those facing in the opposite direction do not. When calculating energies for a complete inhibitor, we accordingly find that pairwise additivity holds more reliably when refinement is started from a protein structure that was pre-built in complex with the fragment that occupies the back-pocket.

Estimating rank of compounds from fragment scores

In the benchmark screening experiments, we ranked five experimentally-validated analogs relative to the rest of the enumerated library. While this was straightforward with smaller libraries, the library built around BDBM50246162 contained almost 300 billion compounds. Determining the precise rank for each active compound would require explicitly counting how many compounds from the library score better/worse than the active analog (a large calculation).

Instead, we instead estimated the rank of each active analog by relying again on the pairwise additivity of the components. For a given analog, we determined the rank of each of the three component fragments relative to all substituents at the corresponding position. For a given fragment, we converted the rank to a percentile (by dividing by the number of fragments), and then to a Z-score by using a standard normal table. Given the independence of the three component fragments, we then summed the Z-scores to yield a Z-score for the complete compound. We then used a standard normal table to convert the latter Z-score to a percentile, which provides an estimate of the proportion of the library that scores ahead of the query (active) compound.

PDB structures used in calculations

Calculations involving structures of the parent inhibitors bound to their cognate kinases were drawn from the corresponding PDB structures: MC180295/CDK9 (PDB: 6W9E), BDBM50091276/CHK1 (PDB:

4RVK), CHIR-124/CHK1 (PDB: 2GDO), BDBM7773/CDK2 (PDB: 1KE7), and BDBM50246162/ACK1 (PDB: 3EQR).

Selectivity calculations across the CDK kinase family were initiated from crystal structures these proteins: CDK1 (PDB: 5LQF), CDK2 (PDB: 4EOQ), CDK5 (PDB: 4AU8), CDK6 (PDB: 2EUF), CDK7 (PDB: 1UA2), CDK8 (PDB: 5IDN), CDK9 (PDB: 3BLQ). Because there were no crystal structure available for CDK3, CDK4, and CDK11, comparative models were generated using SWISS-MODEL [76] for these (using PDB templates 4EOR, 1XO2, and 6GUE, respectively).

Screens were carried out against the inhibitor-bound kinases, and also structures solved with a nucleotide (ATP/ADP/AMP/etc.) rather than an inhibitor. The nucleotide-bound structures used in these screens were: MC180295/CDK9 (PDB: 4IMY), BDBM50091276/CHK1 (PDB: 7AKM), CHIR-124/CHK1 (PDB: 7AKM), BDBM7773/CDK2 (PDB: 2CCH), and BDBM50246162/ACK1 (PDB: 1U54).

Acknowledgements

This work used the Extreme Science and Engineering Discovery Environment (XSEDE) allocation MCB130049, which is supported by National Science Foundation grant number ACI-1548562. This work was supported by grants from the National Institute of General Medical Sciences (R01GM123336) and from the National Science Foundation (CHE-1836950). This research was funded in part through the NIH/NCI Cancer Center Support Grant P30CA006927.

Supplemental Tables

Library	Internal library name	SMARTS string to search PubChem for suitable building blocks	SMARTS string to generate fragments from the resulting building blocks (i.e., by linking onto the hinge-binding core)
MC180295	R1	[H]C([H])(Br)[#6](=O)-[#6]-1=[#6]-[#6]=[#6]-[#6]=[#6]-1	[#6:4]-[#6:2](=[O:1])-[#6:3]Br>>[#6:4]-[#6:2](=[O:1])-[#6:3]-1=[#6](-[#7])-[#7]=[#6](-[#7])-[#16]-1
	R2	[H][#7]([H])-*	[#6:1]-[#7H2:2]>>[#6:1]-[#7:2]-[#6]-1=[#7]-[#6](-[#7])=[#6]-[#16]-1
	R1_R2		[#6:6]-[#6:2](=[O:1])-[#6:3]Br.[#6:5]-[#7H2:4]>>[#6:5]-[#7:4]-[#6]-1=[#7]-[#6](-[#7])=[#6:3](-[#16]-1)-[#6:2](-[#6:6])=[O:1]
BDBM50091276	R1	[H][#7]([H])-[#6]-1=[#6](I)-[#6]=[#6]-[#7]=[#6]-1	[#7:6]-[#6:5]-1=[#6:7]-[#7:1]=[#6:2]-[#6:3]=[#6:4]-1I>>[#7:6]-1-[#6:5]-2=[#6:4](-[#6:3]=[#6:2]-[#7:1]=[#6:7]-2)-[#6]-2=[#6]-1-[#7]=[#6]-[#6]=[#6]-2
	R2	[H][#8]-[#5](-[*,#1])-[#8][H]	[#8]-[#5](-[#8])-[*:1]>>[*:1]-[#6]-1=[#6]-[#6]-2=[#6](-[#7]-[#6]-3=[#6]-[#7]=[#6]-[#6]=[#6]-2-3)-[#7]=[#6]-1
	R1_R2		[#7:2]-[#6:3]-1=[#6:4]-[#7:5]=[#6:6]-[#6:7]=[#6:8]-1I.[#8]-[#5](-[#8])-[*:1]>>[*:1]-[#6]-1=[#6]-[#6]-2=[#6](-[#7:2]-[#6:3]-3=[#6:8]-2-[#6:7]=[#6:6]-[#7:5]=[#6:4]-3)-[#7]=[#6]-1
CHIR-124	R1	[H][#7]-1-[#6](=O)-[#8]-[#6](=O)-[#6]-2=[#6]-1-[#6]=[#6]-[#6]=[#6]-2	[O:6]=[#6:5]-1-[#6:7]~[#6:8]-[#7:1]-[#6:2](=[O:3])-[#8:4]-1>>[O:3]=[#6:2]-1-[#7:1]-[#6:8]~[#6:7]-[#6:5]=[#6:4]-1
	R2	[H][#7]-1-[#6]-2=[#6](-[#6]=[#6]-[#6]=[#6]-2)-[#7]=[#6]-1C([H])([H])[#6](=O)-[#8]C([H])([H])C([H])([H])[H]	[#6]-[#6]-[#6]-[#8]-[#6:3](=[O:4])-[#6:2]-[*:1]>>[*:1]-[#6:2]-1=[#6]-[#6]-2=[#6]-[#6]=[#6]-[#6]=[#6]-2-[#7]-[#6:3]-1=[O:4]
	R1_R2		[O:6]=[#6:5]-1-[#6:7]~[#6:8]-[#7:1]-[#6:2](=[O:3])-[#8:4]-1.[#6]-[#6]-[#6]-[#8]-[#6](=O)-[#6]-[*:9]>>[*:9]-[#6:4]-1=[#6:5]-[#6:7]~[#6:8]-[#7:1]-[#6:2]-1=[O:3]
BDBM7773	R1	[H][#7]([H])-[#6]-1=[#6]-[#6]=[#6]-[#6]=[#6]-1	[#7:1]-[#6:2]-1=[#6:3]-[#6:4]=[#6:5]-[#6:6]=[#6:7]-1>>[#7]\[#6]=[#6]-1\[#6](=O)-[#7:1]-[#6:2]-2=[#6:3]-[#6:4]=[#6:5]-[#6:6]=[#6:7]-1-2
	R2	[H][#7]([H])-*	[#7:1]-[*:2]>>[*:2]-[#7:1]\[#6]=[#6]-1/[#6](=O)-[#7]-[#6]-2=[#6]-[#6]=[#6]-[#6]=[#6]-1-2
	R1_R2		[#7:1]-[#6:2]-1=[#6:3]-[#6:4]=[#6:5]-[#6:6]=[#6:7]-1.[#7:8]-[*:9]>>[*:9]-[#7:8]\[#6]=[#6]-1/[#6](=O)-[#7:1]-

			[#6:2]-2=[#6:3]-[#6:4]=[#6:5]-[#6:6]=[#6:7]-1-2
BDBM50246162	R1	[H][#7]([H])-*	[#7:2]-[*:1]>>[#7]-[#6]-1=[#7]-[#6]=[#6]-2-[#6](-[#7:2]-[*:1])=[#7]-[#7]-[#6]-2=[#7]-1
	R2	[H][#7]([H])-[#7]([H])-*	[#7:1]-[#7:2]-[*:3]>>[#7]-[#6]-1=[#7:1]-[#7:2](-[*:3])-[#6]-2=[#7]-[#6](-[#7])=[#7]-[#6]=[#6]-1-2
	R3	[H][#7]([H])-*	[#7:2]-[*:1]>>[#7]-[#6]-1=[#7]-[#7]-[#6]-2=[#7]-[#6](-[#7:2]-[*:1])=[#7]-[#6]=[#6]-1-2
	R1_R2_R3		[#7:2]-[*:1].[#7:3]-[#7:4]-[*:5].[#7:7]-[*:6]>>[*:1]-[#7:2]-[#6]-1=[#7:3]-[#7:4](-[*:5])-[#6]-2=[#7]-[#6](-[#7:7]-[*:6])=[#7]-[#6]=[#6]-1-2

Table S1: SMARTS templates for transforming building blocks into libraries. The R1 and R2 SMARTS strings encode the reactions needed to transform building blocks into the corresponding fragments (i.e., by adding the hinge-binding scaffold). The R1_R2 SMARTS strings encode all at once the complete set of reactions needed to transform multiple building blocks into the final inhibitor.

Option	Value
Single or double bonds match aromatic bonds	True
Chain bonds in the query may match rings in hits	True
Atoms must be of the specified isotope	True
Allow match to tautomers of the given structure	True
Atoms must match the specified charge	False
Rings may not be embedded in a larger system	False
Remove any explicit hydrogens before searching	False

Table S2: Search parameters for identifying building blocks in PubChem, using SMARTS matching.

AA BLOCKS	Ambinter	Chemhere	Sigma-Aldrich
ABI Chem	Aurora Fine Chemicals LLC	ChemTik	SynHet - Synthetic Heterocycles
AKos Consulting & Solutions	BLD Pharm	Enamine	TimTec
Alichem	ChemBridge	Life Chemicals	Vitas-M Laboratory
Ambeed	ChemDiv	MuseChem	

Table S3: Vendors included in our search for available building blocks.

References

1. Kontoyianni M. Docking and Virtual Screening in Drug Discovery. *Methods Mol Biol*. 2017; 1647:255-66.

2. Jorgensen WL. Efficient drug lead discovery and optimization. *Acc Chem Res*. 2009; 42:724-33.

3. Cournia Z, Allen B, Sherman W. Relative Binding Free Energy Calculations in Drug Discovery: Recent Advances and Practical Considerations. *J Chem Inf Model*. 2017; 57:2911-37.

4. Irwin JJ, Shoichet BK. ZINC--a free database of commercially available compounds for virtual screening. *J Chem Inf Model*. 2005; 45:177-82.

5. Irwin JJ, Sterling T, Mysinger MM, Bolstad ES, Coleman RG. ZINC: a free tool to discover chemistry for biology. *J Chem Inf Model*. 2012; 52:1757-68.

6. Wang L, Wu Y, Deng Y, Kim B, Pierce L, Krilov G, Lupyan D, Robinson S, Dahlgren MK, Greenwood J, Romero DL, Masse C, Knight JL, Steinbrecher T, Beuming T, Damm W, Harder E, Sherman W, Brewer M, Wester R, Murcko M, Frye L, Farid R, Lin T, Mobley DL, Jorgensen WL, Berne BJ, Friesner RA, Abel R. Accurate and reliable prediction of relative ligand binding potency in prospective drug discovery by way of a modern free-energy calculation protocol and force field. *J Am Chem Soc*. 2015; 137:2695-703.

7. Lyu J, Wang S, Balius TE, Singh I, Levit A, Moroz YS, O'Meara MJ, Che T, Algaa E, Tolmachova K, Tolmachev AA, Shoichet BK, Roth BL, Irwin JJ. Ultra-large library docking for discovering new chemotypes. *Nature*. 2019; 566:224-9.

8. Koes D, Khoury K, Huang Y, Wang W, Bista M, Popowicz GM, Wolf S, Holak TA, Domling A, Camacho CJ. Enabling large-scale design, synthesis and validation of small molecule protein-protein antagonists. *PLoS One*. 2012; 7:e32839.

9. Adeshina YO, Deeds EJ, Karanicolas J. Machine learning classification can reduce false positives in structure-based virtual screening. *Proc Natl Acad Sci U S A*. 2020; 117:18477-88.

10. Ghose AK, Herbertz T, Pippin DA, Salvino JM, Mallamo JP. Knowledge based prediction of ligand binding modes and rational inhibitor design for kinase drug discovery. *J Med Chem*. 2008; 51:5149-71.

11. Miduturu CV, Deng X, Kwiatkowski N, Yang W, Brault L, Filippakopoulos P, Chung E, Yang Q, Schwaller J, Knapp S, King RW, Lee JD, Herrgard S, Zarrinkar P, Gray NS. High-throughput kinase profiling: a more efficient approach toward the discovery of new kinase inhibitors. *Chem Biol*. 2011; 18:868-79.

12. Akritopoulou-Zanze I, Hajduk PJ. Kinase-targeted libraries: the design and synthesis of novel, potent, and selective kinase inhibitors. *Drug Discov Today*. 2009; 14:291-7.

13. Chen H, Zhou X, Wang A, Zheng Y, Gao Y, Zhou J. Evolutions in fragment-based drug design: the deconstruction-reconstruction approach. *Drug Discov Today*. 2015; 20:105-13.

14. Pallesen JS, Narayanan D, Tran KT, Solbak SMO, Marseglia G, Sorensen LME, Hoj LJ, Munafo F, Carmona RMC, Garcia AD, Desu HL, Brambilla R, Johansen TN, Popowicz GM, Sattler M, Gajhede M, Bach A. Deconstructing Noncovalent Kelch-like ECH-Associated Protein 1 (Keap1) Inhibitors into Fragments to Reconstruct New Potent Compounds. *J Med Chem*. 2021.

15. Lamoree B, Hubbard RE. Current perspectives in fragment-based lead discovery (FBLD). *Essays Biochem*. 2017; 61:453-64.

16. Kirsch P, Hartman AM, Hirsch AKH, Empting M. Concepts and Core Principles of Fragment-Based Drug Design. *Molecules*. 2019; 24.

17. Bhullar KS, Lagaron NO, McGowan EM, Parmar I, Jha A, Hubbard BP, Rupasinghe HPV. Kinase-targeted cancer therapies: progress, challenges and future directions. *Mol Cancer*. 2018; 17:48.

18. Roskoski R, Jr. Properties of FDA-approved small molecule protein kinase inhibitors. *Pharmacol Res*. 2019; 144:19-50.

19. Taylor SS, Kornev AP. Protein kinases: evolution of dynamic regulatory proteins. *Trends Biochem Sci*. 2011; 36:65-77.

20. Modi V, Dunbrack RL, Jr. Defining a new nomenclature for the structures of active and inactive kinases. *Proc Natl Acad Sci U S A*. 2019; 116:6818-27.

21. Coley CW, Rogers L, Green WH, Jensen KF. Computer-Assisted Retrosynthesis Based on Molecular Similarity. *ACS Cent Sci*. 2017; 3:1237-45.

22. Liu B, Ramsundar B, Kawthekar P, Shi J, Gomes J, Luu Nguyen Q, Ho S, Sloane J, Wender P, Pande V. Retrosynthetic Reaction Prediction Using Neural Sequence-to-Sequence Models. *ACS Cent Sci*. 2017; 3:1103-13.

23. Coley CW, Green WH, Jensen KF. Machine Learning in Computer-Aided Synthesis Planning. *Acc Chem Res*. 2018; 51:1281-9.

24. Lee AA, Yang Q, Sresht V, Bolgar P, Hou X, Klug-McLeod JL, Butler CR. Molecular Transformer unifies reaction prediction and retrosynthesis across pharma chemical space. *Chem Commun (Camb)*. 2019; 55:12152-5.

25. Genheden S, Thakkar A, Chadimova V, Reymond JL, Engkvist O, Bjerrum E. AiZynthFinder: a fast, robust and flexible open-source software for retrosynthetic planning. *J Cheminform*. 2020; 12:70.

26. Shibukawa R, Ishida S, Yoshizoe K, Wasa K, Takasu K, Okuno Y, Terayama K, Tsuda K. CompRet: a comprehensive recommendation framework for chemical synthesis planning with algorithmic enumeration. *J Cheminform*. 2020; 12:52.

27. Lin K, Xu Y, Pei J, Lai L. Automatic retrosynthetic route planning using template-free models. *Chemical Science*. 2020; 11:3355-64.

28. Daylight Theory: SMARTS - A Language for Describing Molecular Patterns. 2020updated 2020; https://www.daylight.com/dayhtml/doc/theory/theory.smarts.html

29. RDKit: Open-source cheminformatics (www.rdkit.org).

30. Bollag G, Hirth P, Tsai J, Zhang J, Ibrahim PN, Cho H, Spevak W, Zhang C, Zhang Y, Habets G, Burton EA, Wong B, Tsang G, West BL, Powell B, Shellooe R, Marimuthu A, Nguyen H, Zhang KY, Artis DR, Schlessinger J, Su F, Higgins B, Iyer R, D'Andrea K, Koehler A, Stumm M, Lin PS, Lee RJ, Grippo J, Puzanov I, Kim KB, Ribas A, McArthur GA, Sosman JA, Chapman PB, Flaherty KT, Xu X, Nathanson KL, Nolop K. Clinical efficacy of a RAF inhibitor needs broad target blockade in BRAF-mutant melanoma. *Nature*. 2010; 467:596-9.

31. Tsai J, Lee JT, Wang W, Zhang J, Cho H, Mamo S, Bremer R, Gillette S, Kong J, Haass NK, Sproesser K, Li L, Smalley KS, Fong D, Zhu YL, Marimuthu A, Nguyen H, Lam B, Liu J, Cheung I, Rice J, Suzuki Y, Luu C, Settachatgul C, Shellooe R, Cantwell J, Kim SH, Schlessinger J, Zhang KY, West BL, Powell B, Habets G, Zhang C, Ibrahim PN, Hirth P, Artis DR, Herlyn M, Bollag G. Discovery of a selective inhibitor of oncogenic B-Raf kinase with potent antimelanoma activity. *Proc Natl Acad Sci U S A*. 2008; 105:3041-6.

32. Steinbrecher TB, Dahlgren M, Cappel D, Lin T, Wang L, Krilov G, Abel R, Friesner R, Sherman W. Accurate Binding Free Energy Predictions in Fragment Optimization. *J Chem Inf Model*. 2015; 55:2411-20.

33. Durrant JD, Amaro RE, McCammon JA. AutoGrow: a novel algorithm for protein inhibitor design. *Chem Biol Drug Des*. 2009; 73:168-78.

34. Hoffer L, Renaud JP, Horvath D. In silico fragment-based drug discovery: setup and validation of a fragment-to-lead computational protocol using S4MPLE. *J Chem Inf Model*. 2013; 53:836-51.

35. Hawkins PC, Skillman AG, Warren GL, Ellingson BA, Stahl MT. Conformer generation with OMEGA: algorithm and validation using high quality structures from the Protein Databank and Cambridge Structural Database. *J Chem Inf Model*. 2010; 50:572-84.

36. Park H, Zhou G, Baek M, Baker D, DiMaio F. Force Field Optimization Guided by Small Molecule Crystal Lattice Data Enables Consistent Sub-Angstrom Protein-Ligand Docking. *J Chem Theory Comput*. 2021; 17:2000-10.

37. Alford RF, Leaver-Fay A, Jeliazkov JR, O'Meara MJ, DiMaio FP, Park H, Shapovalov MV, Renfrew PD, Mulligan VK, Kappel K, Labonte JW, Pacella MS, Bonneau R, Bradley P, Dunbrack RL, Jr., Das R, Baker D, Kuhlman B, Kortemme T, Gray JJ. The Rosetta All-Atom Energy Function for Macromolecular Modeling and Design. *J Chem Theory Comput*. 2017; 13:3031-48.

38. Zhang H, Pandey S, Travers M, Sun H, Morton G, Madzo J, Chung W, Khowsathit J, Perez-Leal O, Barrero CA, Merali C, Okamoto Y, Sato T, Pan J, Garriga J, Bhanu NV, Simithy J, Patel B, Huang J, Raynal NJ, Garcia BA, Jacobson MA, Kadoch C, Merali S, Zhang Y, Childers W, Abou-Gharbia M, Karanicolas J, Baylin SB, Zahnow CA, Jelinek J, Grana X, Issa JJ. Targeting CDK9 Reactivates Epigenetically Silenced Genes in Cancer. *Cell*. 2018; 175:1244-58 e26.

39. Kirubakaran P, Morton G, Zhang P, Zhang H, Gordon J, Abou-Gharbia M, Issa J-PJ, Wu J, Childers W, Karanicolas J. Comparative Modeling of CDK9 Inhibitors to Explore Selectivity and Structure-Activity Relationships. *bioRxiv*. 2020:10.1101/2020.06.08.138602.

40. Gazzard L, Williams K, Chen H, Axford L, Blackwood E, Burton B, Chapman K, Crackett P, Drobnick J, Ellwood C, Epler J, Flagella M, Gancia E, Gill M, Goodacre S, Halladay J, Hewitt J,

Hunt H, Kintz S, Lyssikatos J, Macleod C, Major S, Medard G, Narukulla R, Ramiscal J, Schmidt S, Seward E, Wiesmann C, Wu P, Yee S, Yen I, Malek S. Mitigation of Acetylcholine Esterase Activity in the 1,7-Diazacarbazole Series of Inhibitors of Checkpoint Kinase 1. *J Med Chem*. 2015; 58:5053-74.

41. Ni ZJ, Barsanti P, Brammeier N, Diebes A, Poon DJ, Ng S, Pecchi S, Pfister K, Renhowe PA, Ramurthy S, Wagman AS, Bussiere DE, Le V, Zhou Y, Jansen JM, Ma S, Gesner TG. 4-(Aminoalkylamino)-3-benzimidazole-quinolinones as potent CHK-1 inhibitors. *Bioorg Med Chem Lett*. 2006; 16:3121-4.

42. Bramson HN, Corona J, Davis ST, Dickerson SH, Edelstein M, Frye SV, Gampe RT, Jr., Harris PA, Hassell A, Holmes WD, Hunter RN, Lackey KE, Lovejoy B, Luzzio MJ, Montana V, Rocque WJ, Rusnak D, Shewchuk L, Veal JM, Walker DH, Kuyper LF. Oxindole-based inhibitors of cyclin-dependent kinase 2 (CDK2): design, synthesis, enzymatic activities, and X-ray crystallographic analysis. *J Med Chem*. 2001; 44:4339-58.

43. Kopecky DJ, Hao X, Chen Y, Fu J, Jiao X, Jaen JC, Cardozo MG, Liu J, Wang Z, Walker NP, Wesche H, Li S, Farrelly E, Xiao SH, Kayser F. Identification and optimization of N3,N6-diaryl-1H-pyrazolo[3,4-d]pyrimidine-3,6-diamines as a novel class of ACK1 inhibitors. *Bioorg Med Chem Lett*. 2008; 18:6352-6.

44. Jencks WP. On the attribution and additivity of binding energies. *Proc Natl Acad Sci U S A*. 1981; 78:4046-50.

45. Barelier S, Cummings JA, Rauwerdink AM, Hitchcock DS, Farelli JD, Almo SC, Raushel FM, Allen KN, Shoichet BK. Substrate deconstruction and the nonadditivity of enzyme recognition. *J Am Chem Soc*. 2014; 136:7374-82.

46. Kramer C, Fuchs JE, Liedl KR. Strong nonadditivity as a key structure-activity relationship feature: distinguishing structural changes from assay artifacts. *J Chem Inf Model*. 2015; 55:483-94.

47. Nasief NN, Hangauer D. Additivity or cooperativity: which model can predict the influence of simultaneous incorporation of two or more functionalities in a ligand molecule? *Eur J Med Chem*. 2015; 90:897-915.

48. Cockroft SL, Hunter CA. Chemical double-mutant cycles: dissecting non-covalent interactions. *Chem Soc Rev*. 2007; 36:172-88.

49. Cavalluzzi MM, Mangiatordi GF, Nicolotti O, Lentini G. Ligand efficiency metrics in drug discovery: the pros and cons from a practical perspective. *Expert Opin Drug Discov*. 2017; 12:1087-104.

50. Larsson A, Jansson A, Aberg A, Nordlund P. Efficiency of hit generation and structural characterization in fragment-based ligand discovery. *Curr Opin Chem Biol*. 2011; 15:482-8.

51. Hopkins AL, Keseru GM, Leeson PD, Rees DC, Reynolds CH. The role of ligand efficiency metrics in drug discovery. *Nat Rev Drug Discov*. 2014; 13:105-21.

52. Ballester PJ. Selecting machine-learning scoring functions for structure-based virtual screening. *Drug Discov Today Technol*. 2019; 32-33:81-7.

53. Chaput L, Martinez-Sanz J, Saettel N, Mouawad L. Benchmark of four popular virtual screening programs: construction of the active/decoy dataset remains a major determinant of measured performance. *J Cheminform*. 2016; 8:56.

54. Lagarde N, Zagury JF, Montes M. Benchmarking Data Sets for the Evaluation of Virtual Ligand Screening Methods: Review and Perspectives. *J Chem Inf Model*. 2015; 55:1297-307.

55. Reau M, Langenfeld F, Zagury JF, Lagarde N, Montes M. Decoys Selection in Benchmarking Datasets: Overview and Perspectives. *Front Pharmacol*. 2018; 9:11.

56. Stein RM, Yang Y, Balius TE, O'Meara MJ, Lyu J, Young J, Tang K, Shoichet BK, Irwin JJ. Property-Unmatched Decoys in Docking Benchmarks. *J Chem Inf Model*. 2021; 61:699-714.

57. Yang Y, Zhang Y, Hua Y, Chen X, Fan Y, Wang Y, Liang L, Deng C, Lu T, Chen Y, Liu H. In Silico Design and Analysis of a Kinase-Focused Combinatorial Library Considering Diversity and Quality. *J Chem Inf Model*. 2020; 60:92-107.

58. Sydow D, Schmiel P, Mortier J, Volkamer A. KinFragLib: Exploring the Kinase Inhibitor Space Using Subpocket-Focused Fragmentation and Recombination. *J Chem Inf Model*. 2020; 60:6081-94.

59. Schneider G, Fechner U. Computer-based de novo design of drug-like molecules. *Nat Rev Drug Discov*. 2005; 4:649-63.

60. Hoffer L, Muller C, Roche P, Morelli X. Chemistry-driven Hit-to-lead Optimization Guided by Structure-based Approaches. *Mol Inform*. 2018; 37:e1800059.

61. Shan J, Pan X, Wang X, Xiao X, Ji C. FragRep: A Web Server for Structure-Based Drug Design by Fragment Replacement. *J Chem Inf Model*. 2020; 60:5900-6.

62. Spiegel JO, Durrant JD. AutoGrow4: an open-source genetic algorithm for de novo drug design and lead optimization. *J Cheminform*. 2020; 12:25.

63. Green H, Koes DR, Durrant JD. DeepFrag: a deep convolutional neural network for fragment-based lead optimization. *Chemical Science*. 2021.

64. Hoffer L, Voitovich YV, Raux B, Carrasco K, Muller C, Fedorov AY, Derviaux C, Amouric A, Betzi S, Horvath D, Varnek A, Collette Y, Combes S, Roche P, Morelli X. Integrated Strategy for Lead Optimization Based on Fragment Growing: The Diversity-Oriented-Target-Focused-Synthesis Approach. *J Med Chem*. 2018; 61:5719-32.

65. Konze KD, Bos PH, Dahlgren MK, Leswing K, Tubert-Brohman I, Bortolato A, Robbason B, Abel R, Bhat S. Reaction-Based Enumeration, Active Learning, and Free Energy Calculations To Rapidly Explore Synthetically Tractable Chemical Space and Optimize Potency of Cyclin-Dependent Kinase 2 Inhibitors. *J Chem Inf Model*. 2019; 59:3782-93.

66. Ghanakota P, Bos PH, Konze KD, Staker J, Marques G, Marshall K, Leswing K, Abel R, Bhat S. Combining Cloud-Based Free-Energy Calculations, Synthetically Aware Enumerations, and Goal-Directed Generative Machine Learning for Rapid Large-Scale Chemical Exploration and Optimization. *J Chem Inf Model*. 2020; 60:4311-25.

67. Gentile F, Agrawal V, Hsing M, Ton AT, Ban F, Norinder U, Gleave ME, Cherkasov A. Deep Docking: A Deep Learning Platform for Augmentation of Structure Based Drug Discovery. *ACS Cent Sci*. 2020; 6:939-49.

68. Ying Y, Kun Y, Matthew P. R, Karl L, Robert A, Brian S, Steven J. Efficient Exploration of Chemical Space with Docking and Deep-Learning2021.

69. Baum B, Muley L, Smolinski M, Heine A, Hangauer D, Klebe G. Non-additivity of functional group contributions in protein-ligand binding: a comprehensive study by crystallography and isothermal titration calorimetry. *J Mol Biol*. 2010; 397:1042-54.

70. Zhou H, Cao H, Skolnick J. FRAGSITE: A Fragment-Based Approach for Virtual Ligand Screening. *J Chem Inf Model*. 2021; 61:2074-89.

71. Ustach VD, Lakkaraju SK, Jo S, Yu W, Jiang W, MacKerell AD, Jr. Optimization and Evaluation of Site-Identification by Ligand Competitive Saturation (SILCS) as a Tool for Target-Based Ligand Optimization. *J Chem Inf Model*. 2019; 59:3018-35.

72. Schuller M, Correy GJ, Gahbauer S, Fearon D, Wu T, Diaz RE, Young ID, Carvalho Martins L, Smith DH, Schulze-Gahmen U, Owens TW, Deshpande I, Merz GE, Thwin AC, Biel JT, Peters JK, Moritz M, Herrera N, Kratochvil HT, Consortium QSB, Aimon A, Bennett JM, Brandao Neto J, Cohen AE, Dias A, Douangamath A, Dunnett L, Fedorov O, Ferla MP, Fuchs MR, Gorrie-Stone TJ, Holton JM, Johnson MG, Krojer T, Meigs G, Powell AJ, Rack JGM, Rangel VL, Russi S, Skyner RE, Smith CA, Soares AS, Wierman JL, Zhu K, O'Brien P, Jura N, Ashworth A, Irwin JJ, Thompson MC, Gestwicki JE, von Delft F, Shoichet BK, Fraser JS, Ahel I. Fragment binding to the Nsp3 macrodomain of SARS-CoV-2 identified through crystallographic screening and computational docking. *Sci Adv*. 2021; 7.

73. Wang L, Chambers J, Abel R. Protein-Ligand Binding Free Energy Calculations with FEP. *Methods Mol Biol*. 2019; 2022:201-32.

74. Lombardo F, Desai PV, Arimoto R, Desino KE, Fischer H, Keefer CE, Petersson C, Winiwarter S, Broccatelli F. In Silico Absorption, Distribution, Metabolism, Excretion, and Pharmacokinetics (ADME-PK): Utility and Best Practices. An Industry Perspective from the International Consortium for Innovation through Quality in Pharmaceutical Development. *J Med Chem*. 2017; 60:9097-113.

75. Fabbro D, Cowan-Jacob SW, Moebitz H. Ten things you should know about protein kinases: IUPHAR Review 14. *Br J Pharmacol*. 2015; 172:2675-700.

76. Waterhouse A, Bertoni M, Bienert S, Studer G, Tauriello G, Gumienny R, Heer FT, de Beer TAP, Rempfer C, Bordoli L, Lepore R, Schwede T. SWISS-MODEL: homology modelling of protein structures and complexes. *Nucleic Acids Res*. 2018; 46:W296-W303.

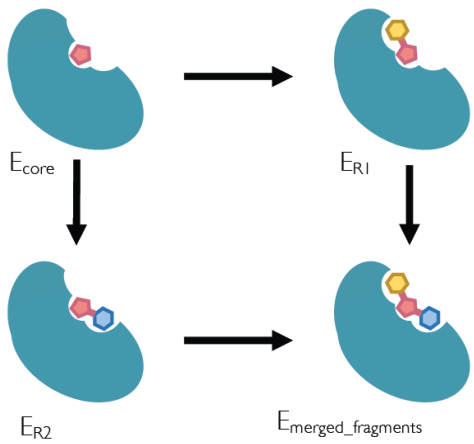

Graphical Abstract